

A CHANDRA X-RAY AND INFRARED STUDY OF THE STELLAR POPULATION IN THE HIGH-MASS STAR FORMING REGION IRAS 16562-3959

VIRGINIE A. MONTES,¹ PETER HOFNER,^{1, 2} LIDIA M. OSKINOVA,³ AND HENDRIK LINZ⁴

¹ Physics Department, New Mexico Institute of Mining and Technology, 801 Leroy Place, Socorro, NM 87801, USA

² Adjunct Astronomer at the National Radio Astronomy Observatory

³ Institute for Physics and Astronomy, University of Potsdam, D-14476 Potsdam, Germany

⁴ Max-Planck-Institute for Astronomy, Königstuhl 17, 69117 Heidelberg, Germany

(Received; Revised; Accepted)

Submitted to The Astrophysical Journal

ABSTRACT

We present the results from Chandra X-ray observations, and near- and mid-infrared analysis, using VISTA/VVV and Spitzer/GLIMPSE catalogs, of the high-mass star-forming region IRAS 16562-3959, which contains a candidate for a high mass protostar. We detected 249 X-ray sources within the ACIS-I field-of-view. The majority of the X-ray sources have low count rates ($< 0.638 \text{ cts/ks}$), and hard X-ray spectra. The search for YSOs in the region using VISTA/VVV and Spitzer/GLIMPSE catalogs resulted in a total of 799 YSOs, with 66 Class I and 733 Class II YSOs. The search for near- and mid-infrared counterparts of the X-ray sources led to a total of 165 VISTA/VVV counterparts, and a total of 151 Spitzer/GLIMPSE counterparts. The infrared analysis of the X-ray counterparts allowed us to add an extra 123 YSOs associated with the region. We conclude that a total of 922 YSOs are associated with the region, with 67 Class I, 764 Class II, and 91 Class III YSOs. We also found that the region is composed of 11 subclusters. In the vicinity of the high-mass protostar, the stellar distribution has a core-halo structure. The subcluster containing the high-mass protostar is the densest and the youngest in the region, and the high-mass protostar is located at its center. The YSOs in this cluster appear to be substantially older than the high mass protostar.

Keywords: open clusters and associations: individual (IRAS 16562-3959) — stars: massive — stars: formation — stars: protostars — stars: pre-main sequence — X-ray: stars — infrared: stars

1. INTRODUCTION

High-mass stars play a dominant role in the physical, chemical, and morphological structure of their host galaxies (e.g. Kennicutt 1998; Cesaroni et al. 2005a), but despite their importance, the formation and early evolution of high-mass stars is still not well understood. The two main theories trying to explain high-mass star formation are the monolithic core accretion model (McKee & Tan 2003) and the competitive accretion model (Bonnell et al. 2001). In the monolithic core accretion model, the physical properties of the molecular core determines the final mass of the star, and it will form in isolation, or in small-N multiple systems. In contrast, in the competitive accretion model, the high-mass star forms at the center of a low-mass stellar cluster, and the mass of the high-mass star is related to the properties of the cluster. See the recent review of Tan et al. (2014) for more details. Characterizing the stellar population associated with high-mass star formation is crucial to decide between the two main theories. Studies of more evolved stellar systems indicate that most high-mass stars are in fact formed in a dense cluster environment (Lada & Lada 2003), but there is a small population of high mass stars which appear to have formed in isolation (de Wit et al. 2005; Oskinova et al. 2013)). As dynamical evolution can significantly change the appearance of a young stellar system, studying early stages of high-mass star formation in young, and hence embedded regions is critical.

Many previous studies of high-mass star forming regions have been carried out at infrared wavelengths (e.g. Lada & Lada 2003) because long wavelengths can penetrate the dust efficiently. However, observing only at infrared wavelengths prevents the detection of YSOs which have partially, or completely lost their circumstellar disk. The Chandra X-ray Observatory allows an alternative view of young stellar populations, as X-ray extinction is low at energies above a few keV, and the background/foreground contamination is relatively small, mainly from nearby stars and AGNs. Furthermore, Classical T Tauri Stars (CTTS) and Weak-line T Tauri Stars (WTTS) are bright in X-rays (Feigelson & Montmerle 1999), and earlier evolutionary phases of YSOs (Class I) are also well known X-ray emitters (Grosso et al. 1997; Neuhäuser & Preibisch 1997). Thus, combining X-ray data with infrared data is an efficient way to study the stellar population in regions where massive stars are forming. In this paper, we present such a study for the high-mass star forming region IRAS 16562-3959, where we have combined Chandra X-ray images and spectra with near- and mid-infrared data from the VISTA/VVV survey, and the Spitzer GLIMPSE survey.

The high-mass protostellar candidate G345.4938+01.4677 associated with IRAS 16562-3959 is located at a distance of 1.7 kpc, and the region has a FIR luminosity of $L = 7 \times 10^4 L_\odot$, clearly indicating the presence of high mass (proto) stars (López et al. 2011). It was discovered by Guzmán et al. (2010) at 6 cm with ATCA, while searching for ionized jets in regions of high FIR luminosity. The 6 cm ATCA data show five aligned continuum sources, where the bright central source presumably indicates the position of the high-mass protostar. The four symmetrically displaced sources have been observed to move away from the central source at high speed (Guzmán et al. 2014), and are likely due to shock-ionization from fast outflowing matter in a jet. IRAS 16562-3959 is also associated with a slower ionized wind, an infalling envelope, and a bipolar molecular outflow, and the mass of the central object has been estimated as $\sim 15 M_\odot$ (Guzmán et al. 2014). Recently, López-Calderon et al. (2016) reported $^{13}\text{CO}(3-2)$ APEX observations of this region, which showed that the high-mass protostellar candidate is located at the column density maximum, further demonstrating its youth.

It is important to point out that while many similar studies have been performed in high-mass star forming regions (e.g. M17, W3, see e.g. Hofner et al. (2002); Townsley et al. (2014)) where HII regions clearly indicate the presence of fully formed massive stars, the IRAS 16562-3959 region contains only a weak radio source which is clearly in a pre-HII region phase of evolution, and is also the only manifestation of high mass star formation within several pc. It thus allows to study the stellar population associated with the formation of a high-mass star in a very early evolutionary phase.

In Section 2, we describe the Chandra observations and data reduction of the region. In Section 3, the X-ray results and analysis of the region are described. A near- and mid-infrared analysis of the region is presented in Section 4. X-ray and infrared source associations are discussed in Section 5. In Section 6, we present a subcluster analysis of the large scale region. In Section 7, we give a discussion of the observational results, and in Section 8 a summary, and general conclusions.

2. CHANDRA X-RAY OBSERVATIONS AND DATA REDUCTION

The IRAS 16562-3959 high-mass star-forming region was observed with the Chandra X-Ray Observatory at three different epochs detailed in Table 1. The first observation (Obs# 1) was made in cycle 14 with an exposure time of 5.02 ks, the second (Obs# 2) and third observations (Obs# 3) were obtained in cycle 16 with exposure times of 38.58 ks

and 40.07 ks respectively, corresponding to a total exposure time of 83.67 ks, i.e. approximately 23 hr. No background flares were detected during these three epochs. The observations were carried out using the imaging array of the Advanced CCD Imaging Spectrometer camera (ACIS-I). ACIS-I consists of four 1024 × 1024 pixel CCDs covering a field-of-view of 17' × 17', and has an energy range from 0.1 to 10 keV. For details on the instrument see Weisskopf et al. (1996, 2002); Garmire et al. (2003). The nominal pointing position used for the three observations was R.A.(J2000) = 16^h59^m41^s.60, Dec.(J2000) = −40°03'43''.6, which are the coordinates of the high-mass protostar (Guzmán et al. 2010). The satellite roll angle (i.e., the angle between the celestial north an the Z-axis of the spacecraft) for Obs#1 was 95.45° and 300.22° for Obs# 2 and 3.

Data reduction was performed using the CIAO software package version 4.7 and CALDB 4.6.8 provided by the Chandra X-ray Center. The data were recalibrated using the *chandra_repro* reprocessing script to create a new level=2 event file and a new bad pixel file for each observation. Before any analysis, it is necessary to correct the absolute astrometry on the three observations. For this, we first used the Obs# 2 data to match Chandra sources with NIR sources from the 2MASS catalog. A set of 23 bright sources were selected in the center of the field-of-view of the ACIS-I array and compared to their 2MASS counterparts. A systematic offset of 0''.1 towards South and 0''.35 toward West was observed. After astrometry correction, the rms offset between Chandra Obs# 2 and 2MASS sources was about 0''.1. Subsequently we corrected the astrometry of Obs# 1 and 3 to match the position of the 23 X-ray sources (when detected) of Obs# 2.

Finally, we filtered the data in three different energy ranges: 0.5 – 2 keV (soft band), 2 – 8 keV (hard band) and 0.5 – 8 keV (full band) and created flux images, exposure maps and PSF maps for each observation and each energy range.

3. X-RAY RESULTS AND ANALYSIS

3.1. Detection

The source identification in the ACIS-I field-of-view was performed using *wavdetect*, a wavelet-based source detection algorithm (Freeman et al. 2002), in three energy ranges: 0.5 – 2 keV (soft band), 2 – 8 keV (hard band) and 0.5 – 8 keV (full band). We used a threshold significance of 10^{-6} corresponding to one spurious source in the field-of-view of ACIS-I, and wavelet scale sizes from 1 to 16 pixels incremented by a factor $\sqrt{2}$. The search was done separately in the three observations and the source lists were joined. Sources with at least 5 counts in the combined observations were considered to be real sources. Due to the large variation of the extinction in the region (our spectral fits imply a range of N_H between $2 \times 10^{21} - 5 \times 10^{23} \text{ cm}^{-2}$; see below), this detection limit corresponds to a range of limiting luminosities of $L_{X,lim} = 2.5 \times 10^{29} - 1.6 \times 10^{32} \text{ erg.s}^{-1}$, for a thermal plasma with $kT = 1 \text{ keV}$.

A total of 249 sources were detected in the field-of-view for the full energy range in the combined three observations, as shown on the flux image in Figure 1. In Obs# 1, a total of 38 sources were detected in the full band, we found 19 sources in the soft band and 20 sources in the hard band. In Obs# 2, a total of 208 sources were detected in the full range of energy, with 102 sources for the soft band and 147 sources for the hard band. In the Obs# 3, a total of 198 sources were detected in the full band, 106 sources were detected in the soft band and 148 sources in the hard band. In Table 2 we list the observed X-ray properties of all our detections. Column (1) lists the source number, column (2) and (3) give the Chandra positions, column (4) is the observed count rate, and column (5) shows the observed X-ray flux. In column (6) we list the hardness ratio for each source defined as $HR = \frac{h_x - s_x}{h_x + s_x}$ where h_x is the count rate in the 2 – 8 keV energy range, and s_x is the count rate in the 0.5 – 2 keV energy range. In column (7) we give the short term variability for each source in each observation, column (8) shows the long term variability of each source, and column (9) lists for each source whether it is variable and which type of variability it shows. Source variability will be discussed in Section 3.2. As expected by studies of stellar X-ray emission in highly embedded clusters at kpc distances, most sources are fairly faint, with approximatively 70 % of the sources having less than 50 counts (count rate 0.638 cts/ks), and according to our hardness ratio classification, the majority of sources have a relatively hard observed X-ray spectrum.

3.2. Timing Analysis and Source Variability

As we have observed this star-forming region at three different epochs, we want to determine if the sources in the field exhibit short-term and/or long-term variabilities. We will refer to changes in count rate of a source within one observation to short term variability. On the other hand, long-term variability corresponds to the overall change in

count rate of a source between observations. A number of physical mechanisms which could explain the different types of variability have been discussed in Flaccomio et al. (2012).

To determine if the sources display short term variability, we first apply the barycenter correction on each observation. Then we compute the fractional area of each source, which creates a correction for instrumental effects, needed for input to the *glvary* tool. Subsequently we ran *glvary* for each individual source, on each observation subdivided into temporal bins of approximate width 2 ks. The *glvary* script uses the Gregory-Loredo variability test algorithm (Gregory & Loredo 1992) which is insensitive to the lightcurve shape and does not overinterpret data in low count rate source as the Kolmogorov-Smirnov (K-S) test could do¹. This test gives us a variability index indicating if the source is variable or not as shown in Table 2 column 7. If the variability index (S.T. Var) is between 0 to 3, it is unlikely that the source is variable. If S.T. Var is 4 or 5, the source may be variable, and if S.T. Var is above 5, the source is definitely variable (Rots 2006).

To determine if the sources have long-term variability, we follow the method from Fridriksson et al. (2008) by computing a significance parameter S (L. T. Var. parameter) for long-term flux variability for each source:

$$S = \frac{|F_{max} - F_{min}|}{\sqrt{\sigma_{F_{max}}^2 + \sigma_{F_{min}}^2}} \quad (1)$$

where F_{max} and F_{min} are the maximum and minimum X-ray count rates during the three observations for each source, and $\sigma_{F_{max}}^2$ and $\sigma_{F_{min}}^2$ are the corresponding errors. A source is defined as long-term variable if $S > 3$. The long-term variability parameter for each source is listed in Table 2 column (8). In Figure 2, we show a sample of sources exhibiting short-term and/or long-term variability.

3.3. Spectroscopy

A spectrum for each source and for each observation was extracted with *srcflux*. To get a single spectrum for each source for all observations, the coadding of the spectra and response files was done using *combine_spectra*. The fitting of each coadded spectrum was then run using Sherpa v1. We used an Absorption \times 1-Temperature model using the *xswabs* and *xsappec* models, with an abundance frozen to 0.3 solar abundance in all cases, which is typical for YSOs (Imanishi et al 2001). Due to the weakness of the sources, we were only able to obtain meaningful fit results for 98 sources, using the following method: after a first initial simultaneous fitting of N_H , T and Emission measure (EM), we kept the fit results if the uncertainties for the parameters were reasonable. This was the case for 6 sources only. If the best model fit showed large uncertainty for the fitted parameters, we froze the fitted value for T and redid the fit. This was the case for 88 sources. In 4 cases the value for the temperature resulted initially in unreasonable high values, and in these cases we assumed and froze a value for T, and fitted for the other parameters. All the fitting results are displayed in Table 3, and sample spectra are shown in Figure 3.

4. INFRARED ANALYSIS OF THE REGION

In order to carry out a more complete analysis of the evolution of the YSO population in the region, we added to our set of X-ray data, all infrared sources detected within a distance of 15' from the high-mass protostar, using mid-infrared ([3.6], [4.5], [5.8] and [8.0] μm) data from the Spitzer/GLIMPSE² (Benjamin et al. 2003) and near-infrared (J, H, and K_s bands) VISTA/VVV³ (Minniti et al. 2010) surveys. A total of 17422 mid-infrared sources were found in the Spitzer/GLIMPSE catalog, and 136183 near-infrared sources were found in the VISTA/VVV catalog. This set of data allows in principle to identify YSOs with disks (Class I and Class II).

To determine foreground and background contamination by star forming galaxies, AGNs, shock emission, and extended PAH emission, as well as which stars are field stars, and which are Class I or II YSOs, we performed the infrared color selection method described in Gutermuth et al. (2009). In Phase I of this method, we used only GLIMPSE sources that have photometry in all four IRAC bands, and have photometric uncertainties $\sigma < 0.2$ mag in all four bands, which corresponds to a total of 2723 sources. In Figure 4 we show Color-Color Diagrams (hereafter CCDs) from the first step of the Phase I selection method, that allowed us to identify contamination from star-forming galaxies and AGNs. Then, we proceeded to the elimination of shock emission and extended PAH emission contamination, as

¹ CIAO manual

² <http://irsa.ipac.caltech.edu/>

³ <http://horus.roe.ac.uk/vsa/>

well as YSO class selection as shown on Figure 5. We ended with a total of 2702 Spitzer/GLIMPSE sources without contamination. We obtained a total of 42 sources classified as Class I, and 176 sources as Class II. We continued with a process similar to the Phase II selection method described by Gutermuth et al. (2009), which we slightly modified due to the use of VISTA/VVV data instead of 2MASS data used in the Gutermuth et al. (2009) paper. In this step, both Spitzer/GLIMPSE and VISTA/VVV data were used. Specifically, the Phase II selection method is applied to Spitzer/GLIMPSE sources that lack [5.8] and/or [8.0] detections. The Spitzer/GLIMPSE sources were first matched with their VISTA/VVV counterparts. We only selected high quality VISTA/VVV detections with $\sigma < 0.1$ mag, and Spitzer/GLIMPSE detections with photometric uncertainties $\sigma < 0.2$ mag in the detected bands for this analysis. A cross-match of both catalogs was done using a search radius of 1'', to create a matched list of 13309 sources. A further selection on these sources was done using their VISTA/VVV magnitudes. We excluded stars with saturated photometry (Soto et al. 2013), by limiting the magnitudes of the detected VISTA/VVV sources to 13.8, 12.8, and 12.8, for J-, H- and K_S-band, respectively. A total of 9974 non-saturated sources were selected. Whenever possible we checked for contamination using similar color-color criteria as described for Phase I, and ended up with a total of 9844 sources without contamination. From these sources, we selected stars exhibiting infrared excess by three different color selection diagrams, as shown in Figure 6. The first selection was done using the CCD J-H vs H-K_S, where we adopted for the slope of the reddening band $\frac{E_{J-H}}{E_{H-K_S}} = 2.02 \pm 0.04$ in the original VISTA system (Soto et al. 2013). Then, we proceeded to a second selection using the CCD J-H vs K_S-[4.5], with the slope of the reddening band $\frac{E_{J-H}}{E_{K_S-[4.5]}} = 2.07$ (Chen et al. 2013). The third color selection was done using the CCD H-K_S vs K_S-[4.5] with the slope of the reddening band $\frac{E_{J-K_S}}{E_{K_S-[4.5]}} = 0.98$ (Chen et al. 2013). A total of 465 infrared excess sources passed all three color selections. To then isolate Class I and Class II YSOs from these infrared excess sources, we used the Phase II color selection from Gutermuth et al. (2009), with the CCD [K_S-[3.6]]₀ vs [[3.6]-[4.5]]₀ as shown in Figure 7. We obtained a total of 24 Class I YSOs and a total of 557 Class II YSOs.

Adding these sources then to what was found in Phase I, the final result of the infrared color selection method for YSOs with disks is a total of 66 Class I YSOs and a total of 733 Class II YSOs.

5. X-RAY AND INFRARED ASSOCIATIONS

5.1. *Infrared Counterparts of the X-Ray Sources*

We searched for near- and mid- infrared counterparts of the 249 detected X-ray sources in the VISTA/VVV and Spitzer/GLIMPSE catalogs. In Figure 8, we show three-color VISTA and Spitzer images of the IRAS 16562-3959 region, on which we have superposed the position of the ACIS array. The astrometric registration between these catalogs is better than 1''. Two different matching radii were used, because of the off-axis Chandra PSF degradation (Getman et al. 2005a). We used 1'' for X-ray sources with off-axis position $\theta \leq 3'$, and the matching radius was enlarged to 2'' for $\theta > 3'$. When several counterparts of the same source were found, we chose the closest counterpart to the X-ray source. We found that 217 of the X-ray sources (87%) have near-infrared counterparts. We selected the J, H and K_S bands, and kept for the analysis only the sources which have good detection in these 3 bands. We ended up with 165 counterparts, which corresponds to 66% of the X-ray sources. The sources and magnitudes are listed in Table 4. Similarly, we found that 151 of the X-ray sources (61%) have mid-infrared counterparts, which are listed with their magnitudes on Table 4. We kept for the analysis all the mid-infrared counterparts having at least one good detection in one of the bands [3.6], [4.5], [5.8] and [8.0] μm . The analysis of the X-ray counterparts in terms of determination of population class and contamination is detailed in Section 4 together with the analysis of all infrared sources detected in the region. The results are presented in Table 4.

5.2. *Selection of Class III YSOs*

We used our X-ray selected VISTA/VVV sources to identify Class III YSOs, by plotting the CCD J-H vs H-K_S shown in Figure 9. Sources defined as Class III YSOs or Weak-line T-Tauri Stars (WTTS) lack substantial warm inner disk material, and are thus considered diskless, but they still could exhibit transitional, or debris disks. They are located in the color space between the two gray dashed lines, where these sources do not exhibit any infrared excess, and thus can be explained by normal reddening. We found a total of 91 Class III YSOs. We also checked that the X-ray sources defined as Class II from the previous analysis are located in the color space defined by the reddened Classical T Tauri Star (CTTS, Class II) locus, and that the Class I sources are located on the right side of the dotted line, corresponding to the Class I color space. From this procedure we found 1 additional Class I YSO,

and 31 additional Class II YSOs. We then proceeded to determine contamination using the color-magnitude diagram (CMD) J vs J-H shown in Figure 9, where the contamination from foreground and background stars is located to the left of the 1 Myr isochrone.

5.3. Unclassified X-Ray Sources

5.3.1. X-ray Sources Without Infrared Counterpart

32 of our detected X-ray sources lack infrared counterparts. We consider two reasons for this. The first one is that those sources are located in regions of high extinction and cannot be detected in the infrared. The second one is that those sources could be extragalactic contamination, in particular AGNs. We consider sources that are located far from regions with high extinction or from the cluster, and that are very faint in X-ray, with count rate lower than 0.638 cts/ks as possible AGN contamination. We also have 3 sources (sources # 1, 226 and 248) that are located far from the cluster, but are very bright in X-ray. These sources are likely galactic contamination, such as X-ray binaries.

5.3.2. X-ray Sources With Infrared Counterparts

5.3.3. subsec:X-ray Sources With Infrared Counterparts

We assume that the X-ray sources that have an incomplete set of infrared data are part of the cluster, and that the poor detection in infrared is due to high extinction. Some of these sources have good detections in the H and K_S band only. A H- K_S color study of our Class II and Class III sources indicates that the H- K_S median for Class II sources is 1.27, and that for Class III sources it is 0.73. Therefore, we classify sources having $H-K_S < 1$ as Class III, and sources having $H-K_S > 1$ as Class II.

6. SUBCLUSTER ANALYSIS

6.1. Membership

Inspecting the images at different wavelength bands (Figures 1 and 8), it is evident that the IRAS 16562-3959 region is not a simple centrally condensed cluster with the massive protostar at its center, but consist of several peak locations where stars have recently formed. In order to investigate the subcluster structure of the region, we have used the k^{th} -nearest neighbor density estimator (kNN) (Casertano & Hut 1985), with $k=18$, to obtain the YSO surface density. The result of this procedure is shown in Figure 10, left panel. We have overlayed on this figure the location of all YSOs as determined in the previous sections. YSO surface density enhancements with the presence of Class I - III YSOs are clearly detected, together with a more uniform distribution of Class II objects. Note however, that our YSO selection method is not sensitive to Class III object outside the ACIS field, i.e. on mid/near-IR data alone.

To further investigate the sub-cluster structure of IRAS 16562-3959, we used the hierarchical density based clustering algorithm HDBSCAN (McInnes et al. 2017), that uses the kNN algorithm, in association with the minimum spanning tree from Prim's algorithm, and hierarchical cluster analysis, to determine the clustering in a dataset (for more details see *How HDBSCAN Works*⁴). The resulting cluster selection from this algorithm is shown in Figure 10, right panel. While there appears to be clustering throughout the region, for further analysis we will concentrate on the clusters that match the YSO density enhancements in Figure 10, left panel, with a threshold of 13 sources pc⁻². We thus selected 11 dense clusters which we have labeled with letters A - K. In Table 5 we give the observed characteristics of each cluster including the name, central position (the median position of all sources in the cluster), the cluster area using a convex hull algorithm which allows to find the smallest polygon that contains a group of discrete points, the radius calculated from the convex hull area, the surface density for each cluster, the total number of YSOs in each cluster and their classification.

It is instructive to compare the subclusters in the IRAS 16562-3959 region with similar objects studied previously. While IRAS 16562-3959 clearly harbors a high-mass protostar which has already developed a luminosity approaching that of O-type ZAMS stars, the subclusters are generally smaller, and contain far less YSOs than similar high mass star forming young clusters, as for instance the regions listed by Getman et al. (2014a). Also, the subcluster structures in these latter regions show a large variation in both size and number of stars compared to the subclusters we have defined above, which are much more uniform in appearance. Our subclusters appear much more similar to the clusters studied by Gutermuth et al. (2009), in terms of physical size, and number of YSOs, and hence also in terms of YSO

⁴ http://hdbSCAN.readthedocs.io/en/latest/how_hdbSCAN_works.html

surface densities. Furthermore, the ratio of the number of Class II and Class I YSOs is similar. Most of the brightest sources in the clusters studied by Gutermuth et al. (2009) have IRAS luminosities below $10^4 L_\odot$, indicating that no massive stars are present.

It is further important to point out the high-mass protostar in IRAS 16562-3959 is located in subcluster H which has the highest observed YSO surface density. We determined a population of 20 YSOs, including the high-mass protostar, which were all detected in X-rays, and only 40% of these have VISTA near-infrared counterparts. Subcluster H has the largest fraction of X-ray sources which were not detected at near- and mid-infrared wavelengths, and thus the most unclassified sources due to extinction. Clearly, the surface density associated with the high-mass protostar, as derived from the IR analysis, needs to be regarded as a lower limit.

6.2. Subcluster X-ray Emission

We have also measured the average X-ray emission per star in each subcluster. We added all counts in each subcluster region, and divided by the sum of the exposure times to derive an average count rate spectrum. These data are shown in Figure 12. Subsequently, we used the same technique to fit the average X-ray spectrum for each subcluster with a thermal spectrum plus one absorption component as described in the section 3.3. The results of the fits are listed in Table 6.

6.3. Age Estimation

In order to estimate the age of each subcluster, we used the Age_{JX} method described in Getman et al. (2014). Specifically we use equations (1) and (2) of that paper to calculate the median age of each subcluster based on its median J-H value. In Table 7 we list for each subcluster (column 1), the number of stars (column 2), the number of stars used in the median age calculation (column 3), the median J-H values (column 4), and the median ages for each subcluster (column 5). The derived ages range bewteen 0.77 Myr (subcluster H) to 1.86 Myr (subcluster D).

We also calculated the disk fraction in each subcluster as follows: $\text{Disk Fraction} = \frac{N_{disk}}{(N_{disk} + N_{diskless})}$, with N_{disk} the number of YSOs with disk (Class I and Class II), and $N_{diskless}$ the number of YSOs without disk (Class III). In Table 7, we list the number of stars used in the disk fraction calculation (column 6), the number of stars with and without disks (columns 7 and 8, respectively), and in column 9 the disk fraction.

7. DISCUSSION

In this study we have attempted to characterize the stellar population in IRAS 16562-3959, in particular with emphasis on the stellar environment of the high-mass protostar located in this region. Inspecting Figure 8, it is clear that IRAS 16562-3959 is located within a much larger region of projected size ≥ 10 pc, and the presence of many young stars in this area indicates that star formation has taken place throughout the region. In particular, there are several young clusters and HII regions toward the south-west of IRAS 16562-3959, demonstrating that high-mass star formation has occurred. Given this morphology, with fully formed high-mass stars located at 2.5 pc to the south-west of a high-mass protostar, one might ask whether triggered star formation has occurred in the region from west toward the east. Considering, however, the ages derived for our subclusters, we see that there is no clear age gradient. For instance, while subcluster H, which contains the high-mass protostar, has in fact the youngest age (0.77 Myr), the two oldest subclusters A and D (1.59 and 1.86 Myr, respectively) are located on opposite sides of subcluster H. Thus, while the high-mass star formation to the south-west could have influenced and perhaps induced star formation in the region, a clear propagation direction is not evident.

The estimates of the ages for the identified subclusters in the region allow us to investigate a number of issues in the star formation history of the region. First, the X-ray analysis presented in this and many similar works profits from the fact that young stars are far more X-ray luminous than main sequence stars. The evolution toward lower X-ray luminosities with time is nicely documented in Figure 4 of Preibisch & Neuhauser (1995), which shows a decrease of median X-ray luminosity from about $10^{30.5} \text{ erg s}^{-1}$ for young clusters to $10^{27.5} \text{ erg s}^{-1}$ for main sequence field stars within a time period of 4 Myr. With our data, we can check whether this trend is also present in the subclusters associated with the IRAS 16562-3959 region. In Figure 13 a), we plot the average X-ray luminosity of each cluster versus age. While there is a large scatter, a trend of decreasing X-ray luminosity with age is clearly visible. Second, many studies have attempted to use the disk fraction determined from NIR photometry as an age indicator (e.g. Haisch, Lada & Lada 2001). However, there appears to be a large spread of ages for disk lifetimes (e.g. Hernández et al. 2008), for a variety of reasons, partly due to observational limitations, and partly due to environmental influences

within the star forming clusters. Hence, considering our Figure 13 b), where we plot the disk fraction versus age, we do not detect a clear correlation. Third, our data allow us to check whether the clusters' stars are unbound, and that the cluster is hence expanding. In Figure 13 c), we plot the stellar surface density versus the age of the subcluster, and again observe a decreasing trend in the surface density with age. In particular, our youngest subcluster H, which contains the high mass protostar, has the highest surface density.

We will now turn to the immediate surroundings of the high-mass protostar G345.4938+01.4677. It is located in subcluster H, which is the youngest and most deeply embedded subcluster in this region. As pointed out above, it also has the highest surface density of young stellar objects, which due to the large extinction toward this subcluster of $N_H \approx 10^{23} \text{ cm}^{-2}$, is only a lower limit. We have detected an X-ray source (source # 161) coincident with the peak of radio continuum emission, which is presumably the position of the high-mass protostar. This emission will be discussed in more detail in a future paper. The position of this object is coincident with the (0,0) position in Figures 10 and 11, and from inspection of Figure 11, it is evident that the high-mass protostar is located near the center of subcluster H. Surrounding subcluster H are subclusters J, E, and G. We note that these three subclusters have ages of about 1 Myr, and all have lower surface densities than subcluster H. We thus find that the high-mass protostar is embedded in a dense cluster, and surrounded with less dense and older distribution of stars, i.e. the stellar distribution can be described as a core-halo structure with an inside-out age gradient.

This result adds to recent findings of similar nature. For instance, a core-halo structure is evident in several clusters studied by Gutermuth et al. (2009), and recently Getman et al. (2014b) reported core-halo age gradients in Orion and NGC 2024. Another example is the study of IRAS 19343+2024 by Ojha et al. (2010): a high-mass protostellar cluster composed of at least four early B-type stars (age $\sim 10^4 - 10^5$ years) surrounded by a rich population of low-mass stars with ages 1 - 3 Myrs. While Getman et al. (2014b) discussed a number of possible scenarios to explain the observed age gradient and core halo structure, the data presented in this work appear to favor the competitive accretion theory for high-mass star formation, where massive stars are expected to form later than the low mass stars in the cluster (Tan et al. 2014).

Finally, it is worthwhile to consider our observational results with reference to a possible observational bias which could influence the judgment of whether the monolithic core accretion scenario of McKee & Tan (2003), or the competitive accretion scenario of Bonnell et al. (2001) is more applicable to the formation of high-mass stars. Candidates for high-mass protostars like the one studied in this paper are often found by deep interferometric radio continuum surveys toward regions of high FIR luminosity, or massive molecular or dust cores. Because such observations are generally dynamic range limited, targets are often chosen from fields which are very radio quiet (e.g. Rosero et al. 2016), i.e. regions which are void of signs of previous high-mass star formation in the form of Ultra-compact or Hyper-compact HII regions. In fact, radio observations of IRAS 16562-3959 show no other detection of radio continuum sources, and hence possible high-mass (proto)stars at very low limits (μJy) within 2 pc (Guzmán et al. (2016), Montes et al. in prep). The early B-type protostar in IRAS 20126+4104 is a similar example (e.g. Hofner et al. 2007). Hence, one might think that this selection method would bias against star formation theories which invoke stellar clusters, and bias toward high-mass stars which might form in isolation. However, the present and other studies (e.g. Montes et al. 2015) demonstrate that also in objects selected in this fashion, an older low-mass stellar cluster is present, indicating that the high-mass protostar may have been the last one to form in the cluster.

8. SUMMARY

We have performed a combined X-ray/infrared study of the young stellar population associated with the high-mass protostellar candidate in IRAS 16562-3959. The main results of this study are:

1) We detected 249 X-ray sources within the Chandra ACIS-I field-of-view. 70% of them have a count rate lower than 0.638 cts/ks. The majority of the sources have a hard X-ray spectrum. We were able to obtain meaningful spectral fit results for 98 sources. The fitted N_H values range from $2.1 \times 10^{21} \text{ cm}^{-2}$ to $4.1 \times 10^{23} \text{ cm}^{-2}$, and the corrected luminosities from $3.9 \times 10^{30} \text{ erg s}^{-1}$ to $7.4 \times 10^{32} \text{ erg s}^{-1}$, meaning that only relatively luminous X-ray sources were detected.

2) Phase I of the infrared analysis, using only the Spitzer/GLIMPSE data, resulted in the identification of 218 YSOs, with 42 Class I and 176 Class II YSOs. Phase II of the infrared analysis, combining Spitzer/GLIMPSE and VISTA/VVV data, yielded 581 YSOs, with 24 Class I and 557 Class II YSOs. Combining the results from Phase I

and Phase II, it was found that a total of 799 YSOs are associated with the region, with 66 Class I, and 733 Class II YSOs.

3) We found that 87% of the X-ray detections (217 sources) have near-infrared counterparts, but only 66% (165 sources) have good detections in the J, H, and K_s bands. We also found that 61% of the X-ray detections (151 sources) have mid-infrared counterparts. The X-ray/infrared analysis resulted in the identification of 91 Class III YSOs. Combining the results of the X-ray/infrared analysis, with the results of the infrared analysis, we conclude that we have a total of 922 YSOs associated with the region, with 67 Class I, 764 Class II, and 91 Class III YSOs.

4) We found that the region is composed of 11 subclusters. We determined the average X-ray luminosity, disk fraction, surface density, and age for each subcluster. We observed a decreasing trend in the average X-ray luminosity with age, no clear correlation between disk fraction and age, and a decreasing trend in the surface density with age. Also, triggered star formation is not evident in the region.

5) In the vicinity of the high-mass protostar, the stellar distribution has a core-halo structure. The subcluster in which the high-mass protostar was formed appears to be the youngest and has the highest surface density. The high-mass protostar (age $\sim 10^5$ years), in its subcluster, is surrounded by older low-mass pre-main sequence stars (age $\sim 10^6$ years), and it is located at the center. The results of the study are compatible with the competitive accretion model of [Bonnell et al. \(2001\)](#).

PH acknowledges support from SAO grants GO3-14005X, and GO5-16008X, as well as partial support from NSF grant AST-0908901 for this work. We thank the New Mexico Institute of Mining and Technology Research Office for their support.

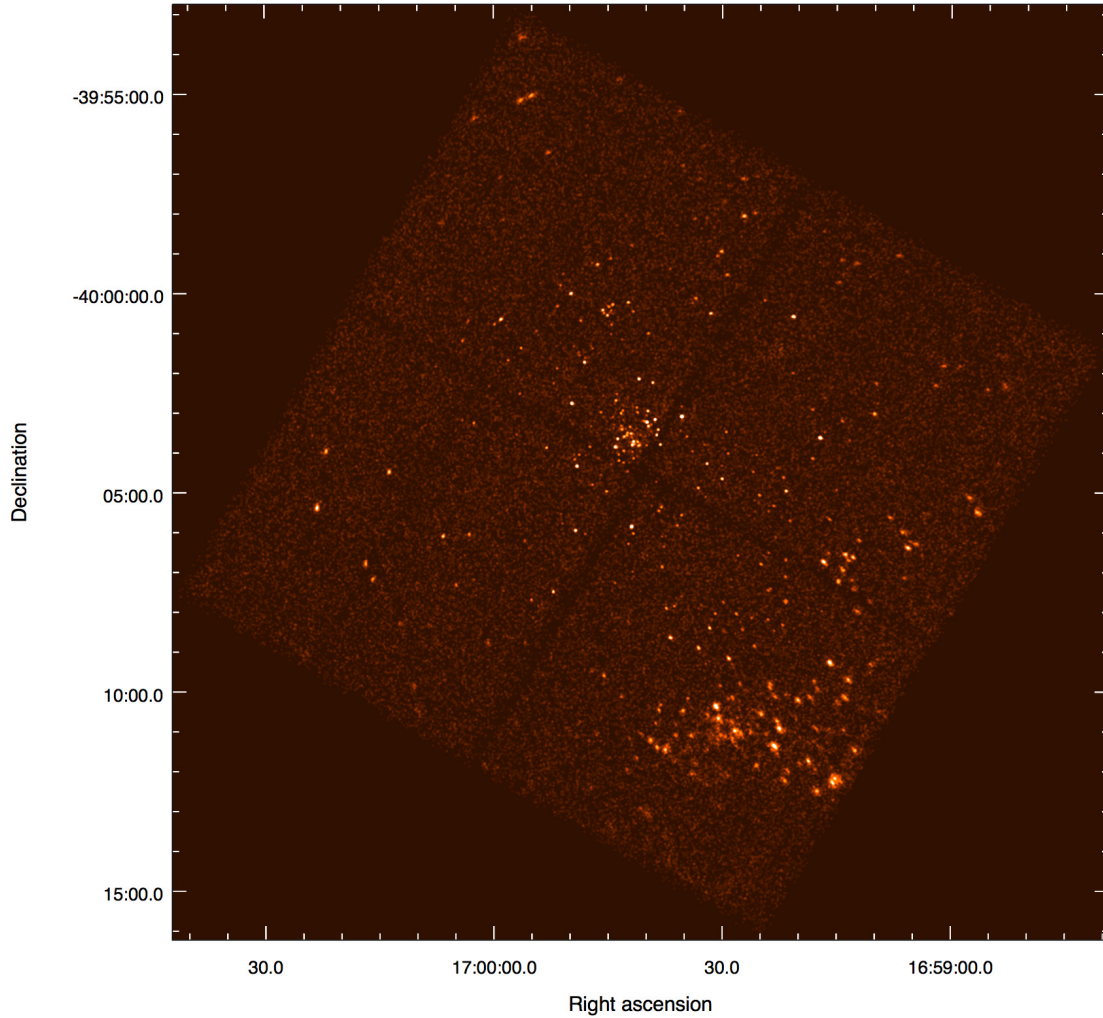


Figure 1. Color image of the three combined observations for the full $17' \times 17'$ ACIS-I field in the $0.5 - 8$ keV band toward IRAS 16562 – 3959. A total of 249 X-ray point sources were detected.

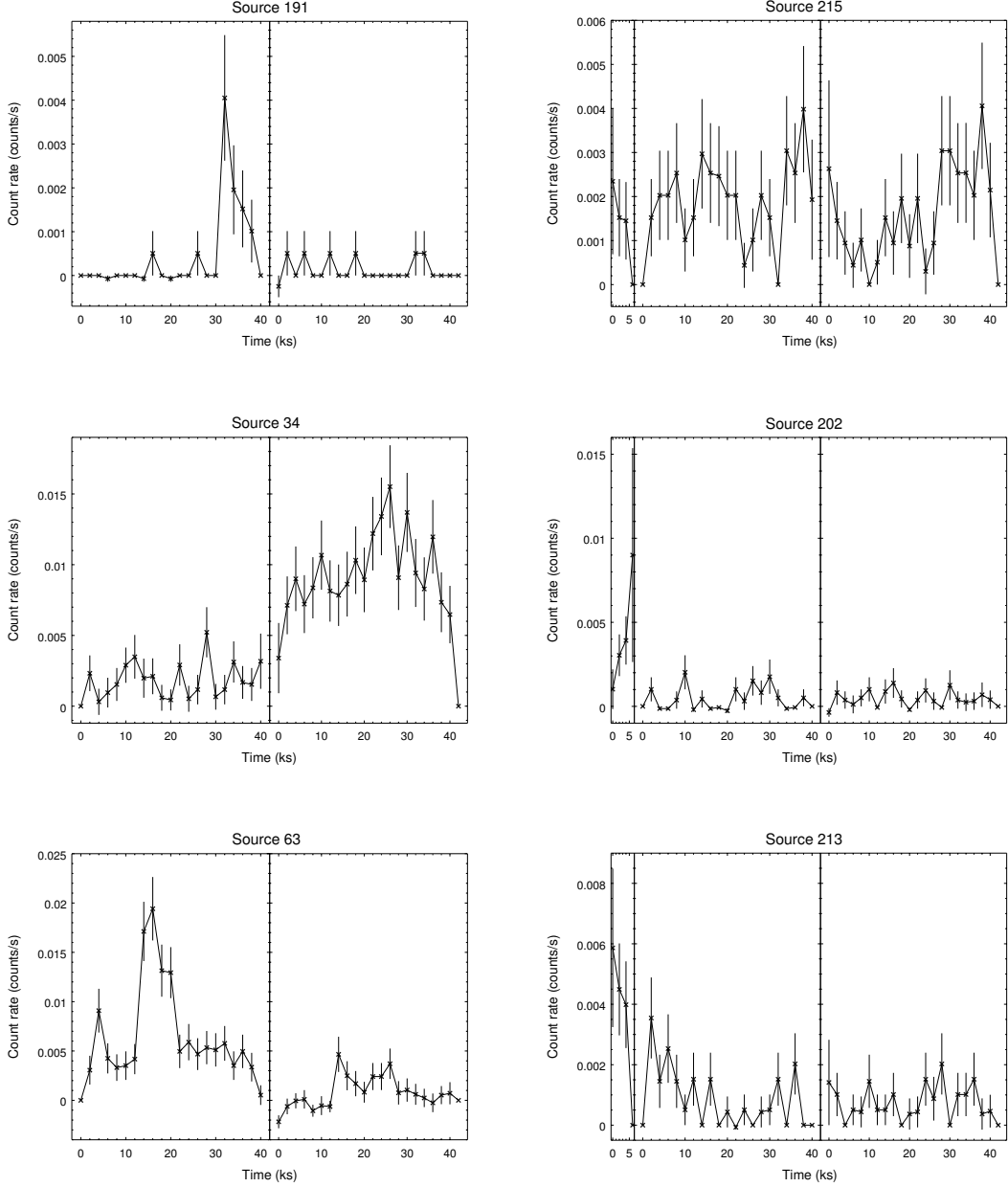


Figure 2. Sample light curves of sources exhibiting short-term and/or long-term variability. The three observations are plotted next to each other. Note that sources on the left panel were not detected in the Obs #1, hence we are only showing the light curves corresponding to Obs #2 and 3. Sources #191 and 215 exhibit short-term variability. For source #191, a flare is observed at the end of Obs #2. Sources #34 and 202 exhibit long-term variability, with markedly increased X-ray activity during Obs #3 for source #34, and in Obs #1 for source #202. Sources #63 and 213 exhibit both short-term and long-term variability. Source #63 shows possible flares in both observations and a higher base X-ray activity in Obs #2. Source #213 shows a short-term variability during Obs #2 and a higher X-ray emission level in Obs #1.

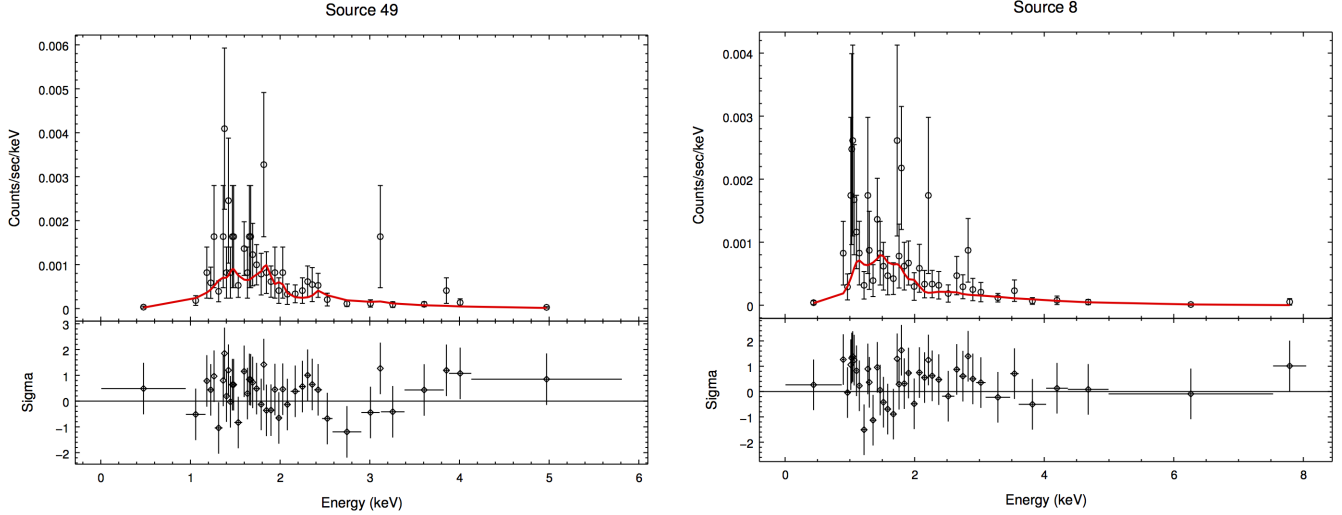


Figure 3. Sample spectra as described in the text. For source #49 we were able to obtain a simultaneous fit of N_H , T, and Emission Measure, whereas for Source #8 the temperature was frozen in the fit.

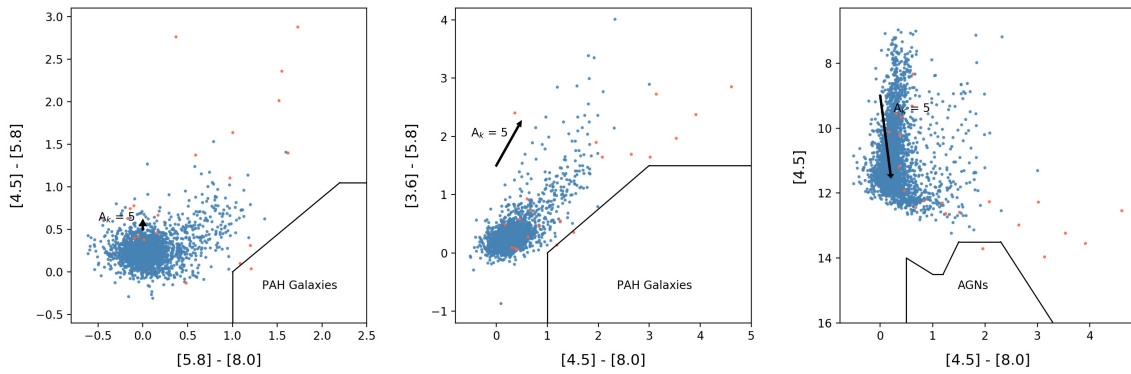


Figure 4. Color-color diagrams (CCDs) used for the determination of the contamination due to star-forming galaxies (left and middle panels); and AGNs (right panel), see Gutermuth et al. (2009) for more details. Orange dots correspond to all contamination found in Phase I; blue dots are field stars.

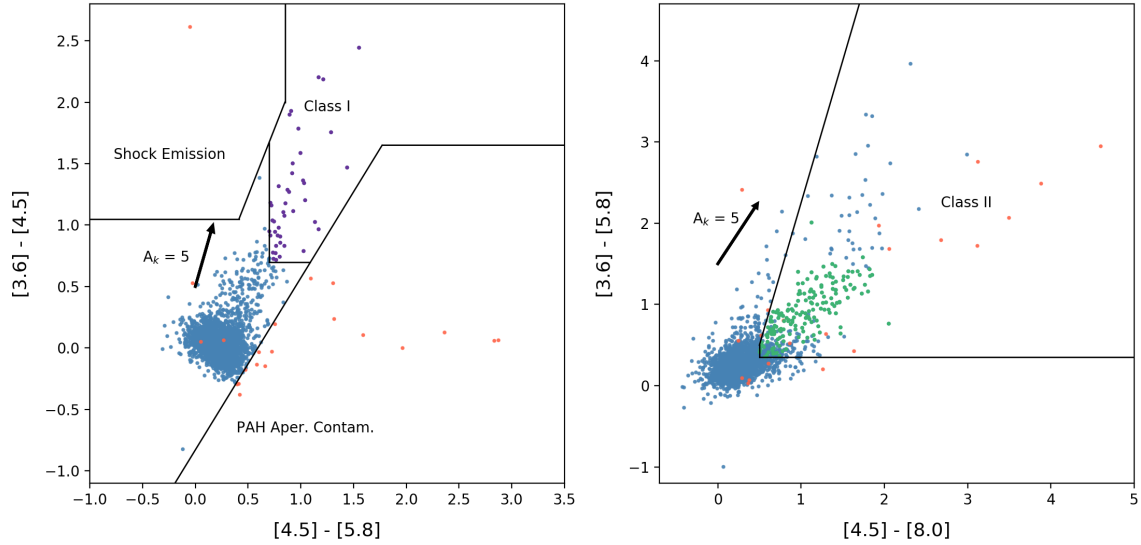


Figure 5. CCDs used to determine contamination and classification of sources. The left panel shows the criteria to isolate unresolved shock emission knots and sources with PAH aperture contamination, and also defines Class I protostars (purple dots). The right panel shows the location of Class II YSOs (green dots). Orange dots correspond to all contamination found in Phase I, blue dots are field stars.

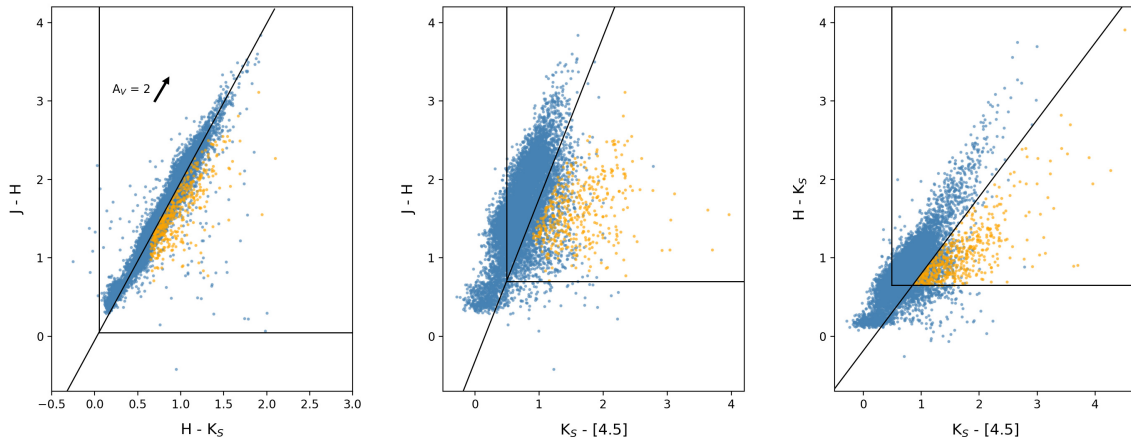


Figure 6. CCDs showing the infrared excess sources selection. The orange dots correspond to the infrared excess sources, and the blue dots correspond to field stars. *Left:* Color-color diagram $J-H$ vs $H-K_S$. The black lines mark the limit for the infrared excess selection with $(J-H) < (H-K_S) \times 2.02 - 0.299$ (Soto et al. 2013), $(J-H) > 0.05$ mag, and $(H-K_S) > 0.05$ mag (Zeilder et al. 2016). *Middle:* CCD $J-H$ vs $K_S-[4.5]$. The black lines mark the limit for the infrared selection with $(J-H) < [(K_S-[4.5])-0.49] \times 2.07 + 0.7$, $(J-H) > 0.7$, and $(K_S-[4.5]) > 0.49$ (Zeilder et al. 2016). *Right:* CCD $H-K_S$ vs $K_S-[4.5]$. The black line mark the limit for the infrared selection with $(H-K_S) < [(K_S-[4.5])-0.49] \times 0.98 + 0.3$, $(H-K_S) > 0.65$, and $(K_S-[4.5]) > 0.49$ (Jose et al. 2016).

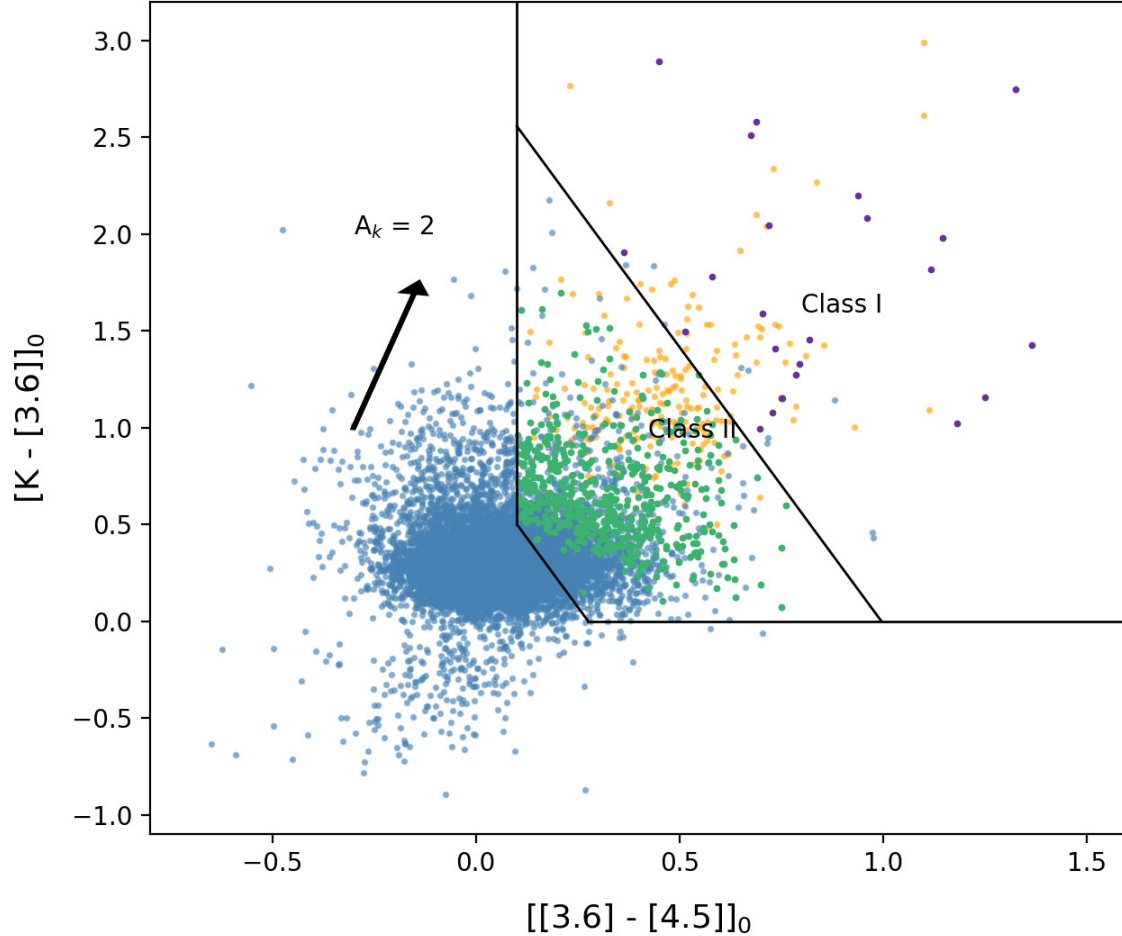


Figure 7. CCD $[K_s - [3.6]]_0$ vs $[[3.6] - [4.5]]_0$ used for the isolation of Class I and Class II YSOs. Purple dots correspond to Class I YSOs, green dots correspond to Class II YSOs, yellow dots are infrared excess sources, and blue dots are field stars.

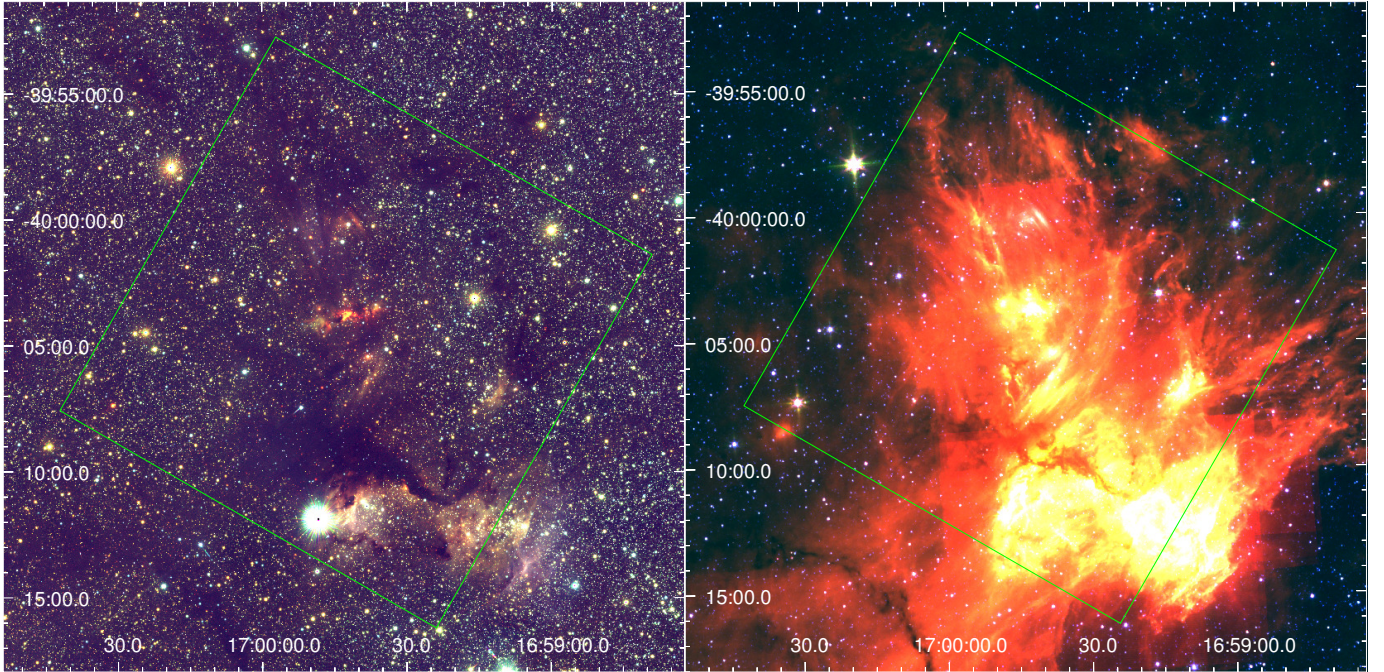


Figure 8. *Left:* VISTA/VVV survey three-color image with J-, H- and K_S-band composite of the IRAS 16562-3959 region. *Right:* Spitzer/GLIMPSE survey three-color image with [3.6], [5.8] and [8.0] bands composite of the IRAS 16562-3959 region. The green square, for both images, indicates the position of the ACIS-I detector.

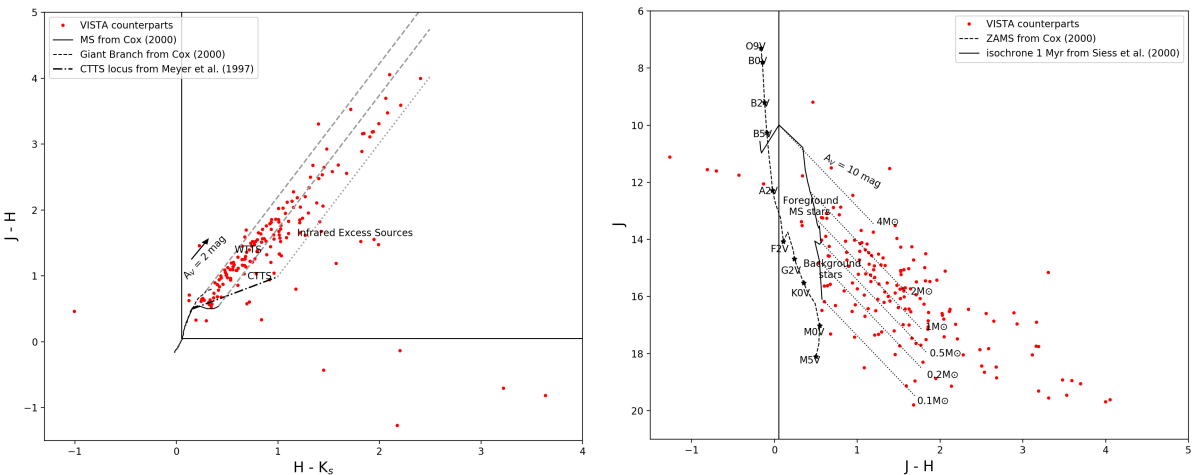


Figure 9. *Left:* CCD J-H vs H-K_S of all X-ray sources having VISTA/VVV counterparts with high-quality photometry. The two straight black lines at (J-H) > 0.05 mag and (H-K_S) > 0.05 mag (Zeilder et al. 2016) mark the limit for the infrared selection. The solid and dashed black line mark the intrinsic color position for main-sequence and giant stars from Cox (2000). The gray dashed lines correspond to the reddening band for main-sequence stars from Rieke & Lebofsky (1985). The dash-dotted line show the locus for CTTS from Meyer et al. (1997), and the dotted line is the reddening band corresponding to the CTTS colors. *Right:* CMD J vs J-H of the same stars as on the left panel. The straight black line at (J-H) > 0.05 mag (Zeilder et al. 2016) mark the limit for the infrared selection. The dashed line indicates the location of the main-sequence stars at the distance to IRAS 16562-3959. The solid black line shows the 1 Myr isochrone from Siess et al. (2000). Dotted lines show the reddening vectors with A_V = 10 mag for different stellar masses.

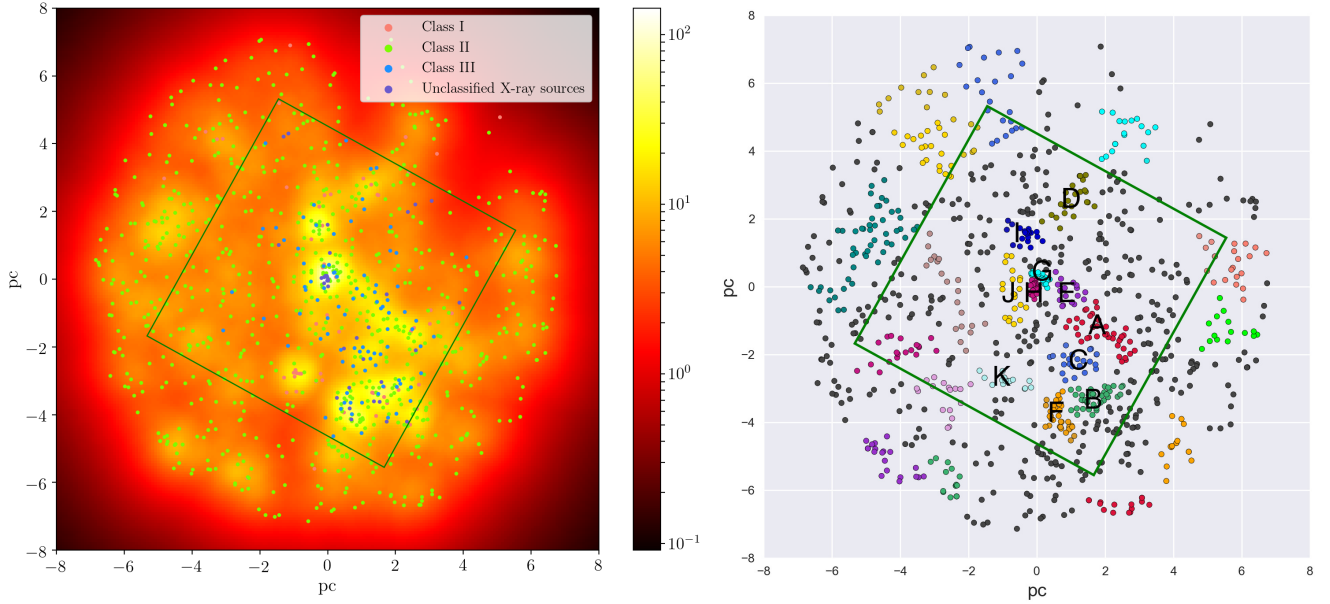


Figure 10. *Left:* Surface density plot for all YSOs considered to be part of the region, with each dot corresponding to a source. Red dots correspond to Class I YSOs, green dots to Class II, blue dots to Class III, and purple dots to unclassified X-ray sources. The units of the colors scale are number of sources per pc^2 . The green square indicates the position of the ACIS-I detector. *Right:* Cluster membership as determined with the HDBSCAN algorithm; each color corresponds to one cluster. The clusters selected for further analysis are denoted by letters.

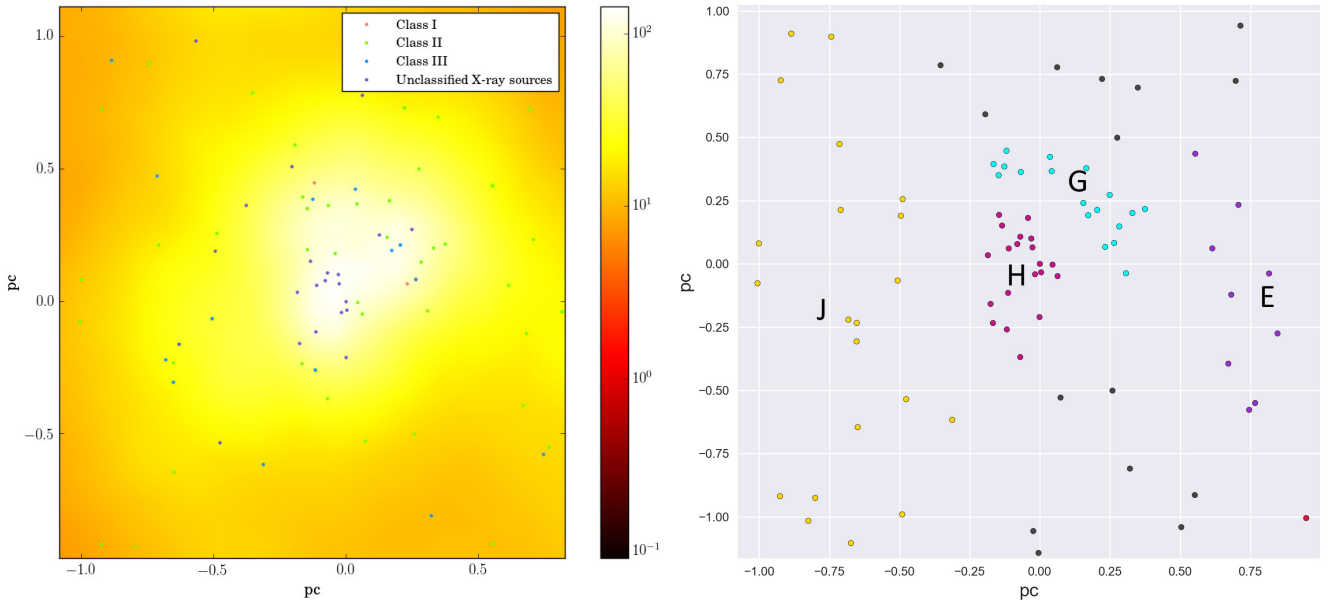


Figure 11. *Left:* Close up of the central cluster from the surface density plot of Figure 10. *Right:* Close up of the central cluster from the cluster membership plot of Figure 10.

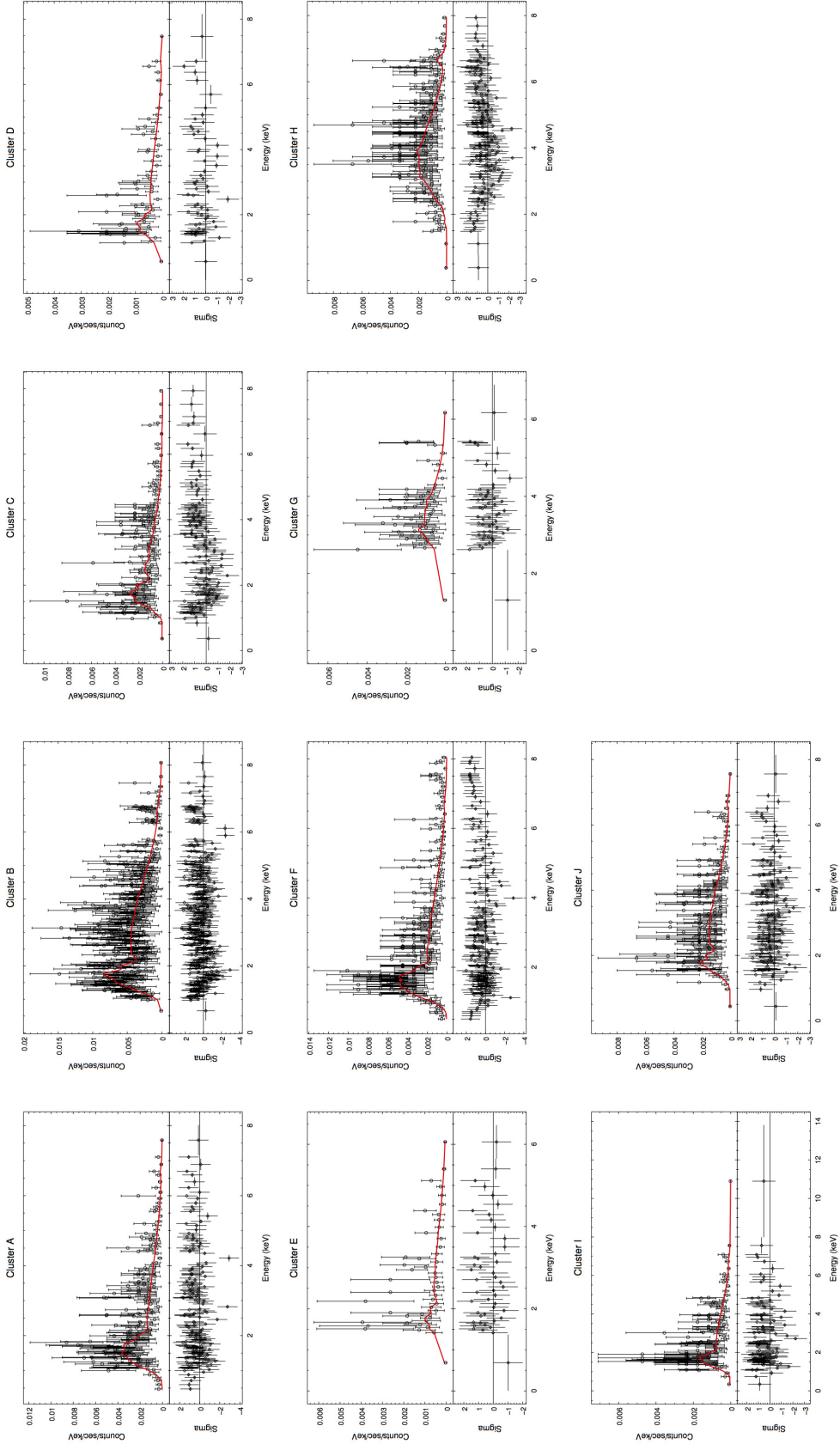


Figure 12. Fitted average X-ray spectra for each subcluster.

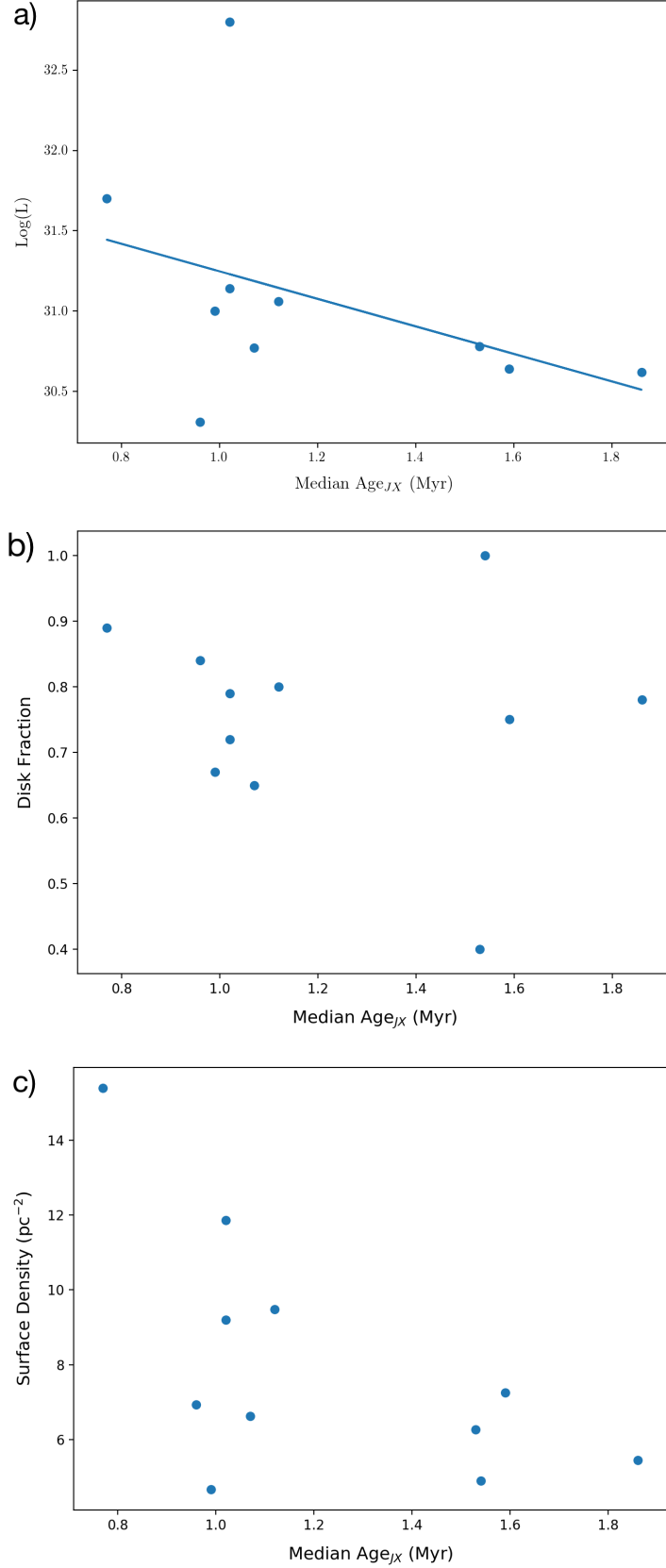


Figure 13. a) Plot of the log of the unabsorbed average luminosity of each subcluster vs. their median age, fitted with a linear regression. b) Plot of the disk fraction calculated for each subcluster vs. their median age. c) Plot of the surface density of each subcluster vs. their median age.

Table 1. Log of Observations

Obs #	Chandra Cycle	ID	Instrument	Exposure	Date	Roll Angle
1	14	ObsID 14537	ACIS-I	5.02 ks	2013 Feb 2	95.45°
2	16	ObsID 16658	ACIS-I	38.58 ks	2015 Jun 30	300.22°
3	16	ObsID 17691	ACIS-I	40.07 ks	2015 Jul 3	300.22°

Table 2. X-Ray Sources

Source #	R.A.	Dec.	Count Rate	F _x	HR	S.T. Var.	L. T.	Var.
	(J2000)	(J2000)	(cts ks ⁻¹)	10 ⁻¹⁴		Index Obs #	Var.	
	(1)	(2)	(3)	(4)	(5)	(6)	(7)	(8)
1	16 58 52.73	-40 02 18.2	0.77	1.28	0.69	... / 6 / 0	1.49	STV
2	16 58 55.13	-40 02 25.4	0.39	0.70	0.75	... / 1 /
3	16 58 56.35	-40 05 30.6	1.75	1.53	-0.31	... / 0 / 0	2.77	...
4	16 58 57.47	-40 05 07.6	0.98	2.57	0.65	... / 1 / 0	0.96	...
5	16 59 01.03	-40 01 50.1	0.44	0.56	-0.77	... / 1 /
6	16 59 01.87	-40 02 17.6	0.47	0.75	0.12	... / ... / 6	...	STV
7	16 59 04.58	-40 06 17.1	0.73	0.65	-0.17	... / 0 / 0	1.11	...
8	16 59 05.59	-40 06 24.0	1.49	1.59	-0.20	... / 6 / 0	0.05	STV
9	16 59 06.05	-40 07 09.4	0.54	0.33	-0.12	... / 0 /
10	16 59 06.13	-40 06 00.4	0.69	1.18	0.35	... / 2 / 0	1.80	...
11	16 59 06.84	-39 59 02.9	0.37	1.04	0.55	... / 0 / 0	0.83	...
12	16 59 08.03	-40 05 36.3	0.41	0.67	0.21	... / 0 / 2	1.35	...
13	16 59 09.73	-40 02 15.8	0.33	0.80	0.66	... / ... / 0
14	16 59 10.03	-40 03 02.5	1.21	2.54	0.70	... / ... / 7	...	STV
15	16 59 10.37	-40 09 19.0	0.87	0.52	-0.19	1 / 2 / ...	2.37	...
16	16 59 10.57	-40 07 43.8	0.26	1.18	0.26	... / ... / 0
17	16 59 12.01	-40 06 12.7	0.41	0.51	-0.21	... / 0 / 0	0.12	...
18	16 59 12.20	-40 07 58.4	0.74	1.40	0.79	... / 0 / 1	2.70	...
19	16 59 12.37	-39 59 14.8	0.47	1.52	0.21	... / 1 /
20	16 59 12.60	-40 11 29.1	1.58	2.57	0.01	1 / 0 / 0	1.52	...
21	16 59 12.74	-40 07 25.5	0.41	1.14	0.36	... / ... / 0
22	16 59 12.75	-40 06 37.9	0.79	1.77	0.69	... / 0 / 8	5.05	STV, LTV
23	16 59 12.96	-40 07 11.5	0.46	0.52	0.56	... / ... / 1
24	16 59 13.42	-40 06 42.3	0.42	0.43	-0.52	... / 0 /
25	16 59 13.47	-40 09 42.1	2.74	6.38	0.67	... / 6 /	STV
26	16 59 13.82	-40 06 34.1	1.12	0.88	-0.47	1 / 0 / 0	2.12	...
27	16 59 13.83	-40 10 09.5	1.21	1.37	-0.30	... / 0 / 0	4.76	LTV
28	16 59 13.99	-40 10 59.2	0.33	0.72	-0.51	... / 0 /
29	16 59 14.19	-40 06 56.9	0.92	0.86	-0.13	0 / 0 / 0	2.05	...
30	16 59 14.21	-40 03 12.3	0.32	0.55	-0.41	... / 0 /
31	16 59 14.23	-39 59 09.6	0.47	1.43	0.69	... / ... / 0
32	16 59 14.70	-40 07 14.3	0.82	1.22	-0.51	... / 0 / 2	2.74	...
33	16 59 14.77	-39 59 42.8	0.40	0.75	0.54	0 / 0 / ...	1.72	...
34	16 59 15.10	-40 12 13.6	5.73	11.86	0.17	... / 0 / 0	14.09	LTV

Table 2 continued on next page

Table 2 (*continued*)

Source #	R.A.	Dec.	Count Rate	F _x	HR	S.T. Var.	L. T.	Var.
	(J2000)	(J2000)	(cts ks ⁻¹)	10 ⁻¹⁴ (erg cm ⁻² s ⁻¹)		Index Obs #		Var.
	(1)	(2)	(3)	(4)	(5)	(6)	1/2/3	Parameter
35	16 59 15.85	-40 09 16.9	3.03	3.05	-0.27	0 / 0 / 0	5.52	LTV
36	16 59 15.91	-40 05 40.7	0.48	1.14	0.13	... / 1 /
37	16 59 16.60	-40 06 45.5	2.19	2.86	0.10	2 / 0 / 7	5.22	STV, LTV
38	16 59 17.12	-40 03 37.9	2.09	2.67	-0.25	... / 2 / 0	0.71	...
39	16 59 17.39	-40 09 57.6	0.51	0.52	-0.31	... / 0 /
40	16 59 17.62	-40 12 30.7	1.52	3.53	0.30	... / 0 / 0	4.90	LTV
41	16 59 17.64	-40 10 54.9	0.58	0.67	-0.59	... / ... / 0
42	16 59 17.85	-40 09 44.3	0.28	0.36	-0.96	... / 0 / 0	0.57	...
43	16 59 18.09	-40 02 54.9	0.39	0.26	0.14	... / ... / 0
44	16 59 18.17	-40 04 08.7	0.32	0.75	0.49	... / 0 / 0	0.69	...
45	16 59 18.45	-40 10 08.9	0.93	1.28	-0.09	... / 2 /
46	16 59 18.63	-40 11 45.2	1.52	2.58	0.48	... / 0 / 0	7.29	LTV
47	16 59 18.63	-40 02 08.6	0.18	0.42	-0.55	... / 0 /
48	16 59 19.99	-40 10 13.7	1.36	2.55	0.33	... / 0 / 6	7.30	STV, LTV
49	16 59 20.65	-40 00 35.2	1.39	1.28	-0.24	0 / 0 / 0	2.67	...
50	16 59 20.71	-40 02 00.4	0.26	0.51	-0.04	... / ... / 1
51	16 59 21.11	-40 05 42.9	0.33	0.30	-0.45	... / 0 /
52	16 59 21.44	-40 11 59.4	0.38	0.47	-0.21	... / 1 / 0	1.47	...
53	16 59 21.48	-40 10 06.0	0.31	0.87	0.62	... / ... / 0
54	16 59 21.62	-40 04 58.2	0.74	0.43	-0.28	0 / 0 / 1	1.13	...
55	16 59 21.63	-40 06 41.7	0.37	0.82	0.04	... / ... / 0
56	16 59 21.68	-40 07 07.5	0.36	0.69	-0.27	... / ... / 2
57	16 59 21.69	-40 07 45.3	0.54	0.73	0.00	... / 1 / 2	2.47	...
58	16 59 21.89	-40 12 13.1	0.93	2.13	0.43	... / 2 / 2	3.76	LTV
59	16 59 21.97	-40 04 37.7	0.22	0.51	0.31	... / 0 / 0	0.32	...
60	16 59 22.11	-40 08 22.2	0.38	0.35	-0.72	... / ... / 0
61	16 59 22.75	-40 10 45.6	3.27	5.94	0.40	... / 2 / 9	4.16	LTV
62	16 59 23.03	-40 10 07.0	0.49	0.63	0.01	... / 2 / 1	0.95	...
63	16 59 23.13	-40 11 22.6	3.86	9.61	0.89	... / 9 / 7	11.01	STV, LTV
64	16 59 23.20	-40 05 20.8	0.17	0.50	0.17	... / 1 / 0	0.60	...
65	16 59 23.69	-40 09 50.6	1.04	1.27	0.54	... / 0 / 0	0.94	...
66	16 59 23.87	-40 05 28.5	0.19	0.54	0.46	... / 2 /
67	16 59 23.93	-40 07 27.8	0.36	0.54	-0.16	... / 1 / 1	1.40	...
68	16 59 23.96	-40 08 11.6	0.18	0.38	-0.21	... / 0 / 0	0.16	...
69	16 59 24.25	-40 11 02.9	0.51	1.92	0.58	... / 1 /
70	16 59 24.37	-40 00 10.9	0.23	1.01	0.56	... / ... / 0
71	16 59 24.76	-40 10 34.2	1.22	1.70	0.35	... / 0 / 0	3.92	LTV
72	16 59 24.87	-40 06 48.3	0.33	0.44	-0.15	... / 1 / 0	1.60	...
73	16 59 25.11	-40 05 04.3	0.34	0.80	0.37	0 / 0 / 1	1.82	...
74	16 59 25.32	-40 02 06.6	0.09	0.00	0.12	... / ... / 1
75	16 59 25.35	-39 57 04.3	0.32	0.41	0.05	... / 0 /
76	16 59 25.39	-40 11 52.4	0.72	1.99	0.15	... / 0 / 0	5.51	LTV
77	16 59 25.50	-40 04 03.6	0.13	0.22	-0.67	... / 1 /
78	16 59 25.67	-40 08 51.8	0.55	0.78	0.14	... / 0 /
79	16 59 25.67	-39 57 59.0	0.34	0.33	0.13	... / 0 / 0	1.52	...
80	16 59 25.94	-40 04 29.3	0.22	0.94	0.52	... / 0 /

Table 2 continued on next page

Table 2 (*continued*)

Source #	R.A.	Dec.	Count Rate	F _x	HR	S.T. Var.	L. T.	Var.
	(J2000)	(J2000)	(cts ks ⁻¹)	10 ⁻¹⁴ (erg cm ⁻² s ⁻¹)		Index Obs #	Var.	
	(1)	(2)	(3)	(4)	(5)	(6)	1/2/3	Parameter
81	16 59 26.10	-40 08 09.0	0.19	0.78	0.14	... / 0 /
82	16 59 26.26	-40 11 01.1	0.32	2.15	0.70	... / 2 /
83	16 59 27.16	-39 58 04.0	1.09	2.36	0.68	... / 0 / 0	6.08	LTV
84	16 59 27.19	-39 57 07.2	0.66	1.48	0.69	... / ... / 0
85	16 59 27.34	-40 08 27.0	0.32	0.78	-0.36	... / 2 /
86	16 59 27.71	-40 09 48.6	0.15	0.44	-0.12	... / ... / 1
87	16 59 27.91	-40 06 35.4	0.18	1.18	0.47	... / 1 /
88	16 59 28.12	-40 08 03.0	0.31	0.34	-0.39	... / 1 / 1	0.28	...
89	16 59 28.32	-40 10 59.2	1.59	3.44	0.78	... / 1 / 0	4.08	LTV
90	16 59 28.73	-40 10 10.3	0.49	0.69	0.54	... / 0 / 0	1.86	...
91	16 59 29.10	-40 09 10.3	1.01	2.76	0.91	0 / 0 / 0	1.04	...
92	16 59 29.39	-39 59 32.5	0.43	0.68	0.05	... / 2 / 0	0.53	...
93	16 59 29.48	-40 03 29.2	0.43	1.72	0.26	... / 6 /	STV
94	16 59 29.78	-40 08 29.0	0.24	0.43	0.11	... / ... / 0
95	16 59 29.83	-40 12 05.1	0.61	0.60	-0.08	... / 0 /
96	16 59 29.85	-40 07 46.4	0.22	0.23	-0.45	... / 1 /
97	16 59 29.99	-40 04 39.9	0.55	1.19	0.54	... / 0 / 1	2.00	...
98	16 59 30.06	-39 58 56.3	0.64	1.43	0.67	1 / 0 / 0	1.74	...
99	16 59 30.19	-40 11 05.7	0.42	1.06	0.20	... / 0 /
100	16 59 30.30	-40 09 52.3	0.44	0.93	0.71	... / 0 /
101	16 59 30.32	-40 12 53.6	0.36	0.89	0.43	... / ... / 0
102	16 59 30.43	-40 10 41.3	1.71	2.79	0.66	... / 0 / 0	1.65	...
103	16 59 30.77	-40 10 22.6	3.38	8.63	0.90	... / 2 / 0	10.58	LTV
104	16 59 30.90	-40 08 02.9	0.23	1.13	0.77	... / 1 / 1	1.07	...
105	16 59 31.52	-40 00 30.7	0.59	1.03	-0.06	0 / 0 / 1	2.60	...
106	16 59 31.63	-40 08 24.6	0.56	0.95	0.04	... / 1 / 2	0.74	...
107	16 59 31.94	-40 07 13.5	0.14	0.55	0.33	... / ... / 0
108	16 59 31.99	-40 04 17.0	0.49	0.67	0.02	... / 1 / 0	1.41	...
109	16 59 32.34	-40 03 48.2	0.15	0.04	-0.54	... / 0 /
110	16 59 32.77	-40 07 49.7	0.16	0.64	-0.06	... / 0 /
111	16 59 33.10	-40 08 53.9	0.73	1.14	0.36	... / 1 / 0	1.04	...
112	16 59 33.14	-40 04 53.7	0.34	0.43	0.52	... / 0 / 0	0.28	...
113	16 59 33.64	-40 11 46.5	0.43	0.74	0.28	... / ... / 0
114	16 59 33.73	-40 12 05.9	0.56	0.71	0.13	... / 0 / 0	2.12	...
115	16 59 33.90	-40 00 15.0	0.37	0.58	0.15	... / 2 / 1	2.47	...
116	16 59 34.04	-40 11 05.8	0.75	1.45	0.38	1 / 1 / 0	1.87	...
117	16 59 34.37	-40 11 25.4	0.35	0.22	0.37	... / 0 / 2	1.45	...
118	16 59 34.49	-40 10 11.5	0.45	1.19	0.48	... / ... / 0
119	16 59 34.64	-40 03 36.2	0.24	0.54	0.52	... / ... / 1
120	16 59 35.21	-40 10 30.1	0.74	0.95	0.21	... / 5 / 0	0.16	STV
121	16 59 35.30	-40 03 05.8	5.80	11.89	0.37	0 / 0 / 0	2.14	...
122	16 59 35.33	-40 02 50.8	0.13	2.05	-0.70	... / 0 /
123	16 59 35.34	-40 05 34.5	0.21	0.59	0.14	... / 2 / 0	0.57	...
124	16 59 35.58	-39 55 26.8	0.26	0.96	0.38	... / 0 / 0	0.61	...
125	16 59 35.89	-40 05 49.9	0.18	0.28	0.17	... / 0 / 0	0.33	...
126	16 59 36.03	-40 10 49.2	0.26	0.44	0.24	... / ... / 0

Table 2 continued on next page

Table 2 (*continued*)

Source #	R.A.	Dec.	Count Rate	F _x	HR	S.T. Var.	L. T.	Var.
	(J2000)	(J2000)	(cts ks ⁻¹)	10 ⁻¹⁴ (erg cm ⁻² s ⁻¹)		Index Obs #	Var.	
	(1)	(2)	(3)	(4)	(5)	(6)	1/2/3	Parameter
127	16 59 36.07	-40 11 05.0	0.40	0.48	-0.41	... / 0 / 2	1.38	...
128	16 59 36.26	-40 07 51.4	0.24	0.64	0.59	... / ... / 1
129	16 59 36.74	-40 08 38.6	1.02	1.51	0.37	... / 0 / 1	5.34	LTV
130	16 59 37.31	-40 07 55.3	0.43	0.76	0.23	0 / 1 / 0	2.03	...
131	16 59 37.35	-40 11 27.5	1.66	1.61	-0.32	... / 6 / 0	2.37	STV
132	16 59 37.70	-40 06 21.8	0.14	0.66	0.33	... / 1 /
133	16 59 37.89	-40 06 52.1	0.25	0.49	0.51	... / 0 / 0	1.89	...
134	16 59 37.97	-40 05 21.9	0.15	0.12	-0.12	... / 0 / 0	1.33	...
135	16 59 38.13	-40 03 48.1	0.50	5.73	0.58	... / 8 /	STV
136	16 59 38.34	-40 05 28.0	0.25	1.46	-0.15	... / 1 /
137	16 59 38.38	-40 10 28.4	0.41	1.20	0.61	... / 0 / 0	0.42	...
138	16 59 38.40	-40 03 25.7	0.46	0.93	0.65	... / 2 / 0	0.78	...
139	16 59 38.55	-40 11 24.8	0.91	0.92	-0.76	... / 1 / 0	0.90	...
140	16 59 38.61	-40 10 48.4	0.44	0.98	0.68	... / 0 /
141	16 59 38.61	-40 03 33.6	0.53	2.07	0.65	... / 7 / 0	3.37	STV, LTV
142	16 59 38.68	-40 04 44.4	0.18	2.31	0.56	... / 2 /
143	16 59 38.79	-40 03 10.6	0.88	1.34	0.64	... / 0 / 1	2.28	...
144	16 59 39.10	-40 02 14.9	0.57	1.01	0.47	1 / 0 / 1	1.56	...
145	16 59 39.30	-40 03 17.8	0.15	0.34	0.49	... / 0 /
146	16 59 39.31	-40 11 13.4	1.10	0.94	-0.57	... / 0 / 0	1.00	...
147	16 59 39.66	-40 03 20.3	0.53	1.05	0.54	... / 0 / 0	2.55	...
148	16 59 39.69	-40 01 00.7	0.27	0.45	0.10	... / 2 / 0	1.86	...
149	16 59 39.74	-40 02 57.7	0.51	0.48	0.16	... / 0 / 1	0.51	...
150	16 59 39.74	-40 13 04.5	1.07	1.04	0.07	... / ... / 0
151	16 59 39.86	-40 03 14.4	1.53	2.08	0.79	... / 0 / 5	7.06	STV, LTV
152	16 59 40.17	-40 03 13.1	0.28	0.47	0.64	... / 0 /
153	16 59 40.60	-40 11 03.2	0.18	0.35	0.46	... / 1 /
154	16 59 40.90	-40 03 49.5	0.29	0.58	0.80	... / 0 / 1	1.08	...
155	16 59 40.92	-40 02 09.3	1.02	2.28	0.93	... / 0 / 1	2.98	...
156	16 59 41.10	-40 03 44.0	0.35	0.98	0.86	... / 0 / 1	0.63	...
157	16 59 41.14	-40 02 59.2	0.17	0.33	0.74	... / 1 / 0	0.46	...
158	16 59 41.21	-40 02 52.3	0.34	0.45	-0.07	... / 0 /
159	16 59 41.25	-40 11 40.9	0.38	0.39	-0.56	... / 0 /
160	16 59 41.56	-40 03 47.7	0.37	1.67	0.71	... / 2 /
161	16 59 41.62	-40 03 43.6	0.89	2.14	0.92	1 / 1 / 2	2.33	...
162	16 59 41.63	-40 04 09.2	0.17	0.55	0.41	... / 5 / 0	0.60	STV
163	16 59 41.65	-40 00 27.8	0.19	0.42	0.68	... / 0 / 0	0.16	...
164	16 59 41.67	-40 06 02.3	0.37	1.77	0.58	... / 7 /	STV
165	16 59 41.74	-40 06 59.7	0.14	0.80	0.31	... / 0 /
166	16 59 41.81	-40 03 48.6	0.51	0.77	0.52	... / 0 / 0	3.37	LTV
167	16 59 41.88	-39 58 47.5	0.25	0.74	0.66	... / ... / 0
168	16 59 41.88	-40 05 51.8	2.90	4.80	0.59	1 / 0 / 0	2.00	...
169	16 59 41.92	-40 03 35.7	0.17	0.28	0.06	... / 1 /
170	16 59 41.96	-40 03 31.5	0.39	1.53	0.78	... / 0 / 1	2.91	...
171	16 59 42.10	-40 03 21.6	0.21	0.40	0.72	... / 1 / 1	1.28	...
172	16 59 42.30	-40 00 14.0	0.46	0.33	-0.86	... / 5 / 1	1.23	STV

Table 2 continued on next page

Table 2 (*continued*)

Source #	R.A.	Dec.	Count Rate	F _x	HR	S.T. Var.	L. T.	Var.
	(J2000)	(J2000)	(cts ks ⁻¹)	10 ⁻¹⁴ (erg cm ⁻² s ⁻¹)		Index Obs #	Var.	
	(1)	(2)	(3)	(4)	(5)	(6)	1/2/3	Parameter
173	16 59 42.31	-40 06 17.5	0.23	0.41	0.26	... / 0 /
174	16 59 42.41	-40 03 30.6	0.24	0.62	0.74	... / 0 / 0	1.86	...
175	16 59 42.41	-40 04 28.3	0.21	1.69	0.60	... / 1 /
176	16 59 42.45	-40 11 58.8	0.48	1.07	0.21	... / 0 /
177	16 59 42.53	-40 03 34.1	0.24	1.09	0.77	... / 0 / 1	0.57	...
178	16 59 42.88	-40 03 36.2	0.44	1.78	0.86	0 / 1 / 0	2.23	...
179	16 59 42.90	-40 03 57.5	0.40	0.82	0.77	... / 1 /
180	16 59 42.95	-40 04 15.1	0.22	2.09	0.49	... / ... / 6	...	STV
181	16 59 43.05	-40 02 56.9	0.36	0.59	0.32	... / ... / 0
182	16 59 43.15	-40 03 25.2	0.46	1.89	0.72	... / 0 /
183	16 59 43.18	-40 10 07.1	0.25	0.28	-1.00	... / ... / 1
184	16 59 43.27	-40 03 20.1	0.20	0.49	0.08	... / 0 /
185	16 59 43.28	-40 03 01.1	0.31	0.44	0.33	... / 0 / 2	1.55	...
186	16 59 43.45	-39 54 38.5	0.46	0.45	-0.51	... / 2 /
187	16 59 43.51	-40 04 12.0	0.27	0.90	0.34	... / 0 / 1	1.75	...
188	16 59 43.61	-40 04 02.8	0.32	1.46	0.76	0 / ... / 0	2.25	...
189	16 59 43.72	-40 03 39.5	1.39	4.37	0.90	... / 8 /	STV
190	16 59 43.82	-40 02 31.9	0.23	0.67	0.27	... / 2 /
191	16 59 43.94	-40 02 42.0	0.31	0.62	0.64	... / 8 / 0	2.67	STV
192	16 59 44.01	-40 03 51.7	0.98	1.19	0.28	... / 1 / 6	0.73	STV
193	16 59 44.09	-40 07 16.6	0.19	0.37	-0.12	... / 0 /
194	16 59 44.35	-40 00 17.2	0.36	0.80	0.14	... / 2 / 0	1.86	...
195	16 59 44.54	-40 00 47.4	0.27	0.27	-0.11	... / 1 /
196	16 59 44.60	-40 00 26.3	0.25	1.00	0.57	... / ... / 0
197	16 59 44.71	-39 59 07.4	0.36	0.59	0.40	... / 1 /
198	16 59 44.84	-40 00 20.6	0.33	0.78	0.44	... / 0 / 0	3.58	LTV
199	16 59 45.09	-40 00 33.5	0.93	1.69	0.37	... / ... / 6	...	STV
200	16 59 45.16	-40 04 58.4	0.24	0.62	0.38	... / 0 / 0	2.17	...
201	16 59 45.51	-40 00 30.3	0.33	0.74	-0.12	... / ... / 0
202	16 59 45.54	-40 09 36.2	0.64	1.01	0.50	2 / 2 / 0	3.56	LTV
203	16 59 45.68	-40 00 25.4	1.03	2.09	0.32	... / ... / 8	...	STV
204	16 59 45.91	-40 02 59.7	0.20	0.51	0.70	... / 1 / 0	3.89	LTV
205	16 59 46.32	-39 59 16.9	0.54	0.70	0.23	... / 1 / 2	1.63	...
206	16 59 47.03	-40 04 48.6	0.25	0.27	0.09	... / ... / 0
207	16 59 47.24	-40 03 20.5	0.17	0.39	0.40	... / ... / 0
208	16 59 47.37	-40 03 51.6	0.17	0.84	0.66	... / 2 / 2	0.60	...
209	16 59 48.06	-40 01 44.2	0.82	1.33	0.74	... / 0 / 6	2.72	STV
210	16 59 48.55	-40 00 41.5	0.39	0.24	-0.44	... / 2 /
211	16 59 48.81	-40 04 03.3	0.22	0.54	0.49	... / 1 /
212	16 59 49.03	-40 04 20.8	1.28	1.40	0.09	... / 5 / 0	6.62	STV, LTV
213	16 59 49.26	-40 05 57.6	1.05	1.34	0.59	1 / 6 / 0	3.51	STV, LTV
214	16 59 49.37	-40 04 10.4	0.26	0.46	0.12	... / ... / 1
215	16 59 49.73	-40 02 46.2	1.78	3.32	0.74	0 / 0 / 6	0.58	STV
216	16 59 49.83	-40 00 00.7	0.89	1.19	-0.21	0 / 2 / 1	3.49	LTV
217	16 59 50.99	-40 05 46.9	0.17	0.43	0.40	... / ... / 3
218	16 59 51.22	-39 59 47.6	0.27	0.62	0.19	... / ... / 2

Table 2 continued on next page

Table 2 (*continued*)

Source #	R.A.	Dec.	Count Rate	F _x	HR	S.T. Var.	L. T.	Var.
	(J2000)	(J2000)	(cts ks ⁻¹)	10 ⁻¹⁴		Index Obs #	Var.	
	(1)	(2)	(3)	(4)	(5)	(6)	1/2/3	Parameter
219	16 59 51.61	-40 00 19.9	0.25	0.48	0.55	... / 0 / 0	1.22	...
220	16 59 51.68	-40 01 53.2	0.15	0.68	0.33	... / ... / 2
221	16 59 52.17	-40 07 30.0	0.62	0.57	-0.86	2 / 0 / 2	1.66	...
222	16 59 52.83	-39 56 28.3	0.61	0.58	-0.45	... / ... / 0
223	16 59 53.04	-40 03 52.9	0.33	0.46	0.62	... / 0 / 7	0.69	STV
224	16 59 54.84	-39 55 01.5	1.25	3.83	0.81	... / 0 / 0	0.95	...
225	16 59 55.03	-40 07 42.1	0.22	0.38	0.01	... / 0 / 2	0.16	...
226	16 59 56.38	-39 53 32.0	1.21	2.71	0.59	... / 0 / 1	1.78	...
227	16 59 56.40	-40 01 22.6	0.25	0.30	-0.83	... / 1 / 1	0.57	...
228	16 59 56.52	-39 55 11.9	0.94	1.40	0.31	... / 2 / 0	4.68	LTV
229	16 59 58.08	-40 01 41.0	0.25	0.82	0.09	... / 0 /
230	16 59 59.00	-40 00 39.0	0.88	2.53	0.93	... / 1 / 0	0.63	...
231	16 59 59.17	-39 57 06.1	0.38	0.40	-0.51	... / ... / 2
232	16 59 59.86	-40 00 46.8	0.28	0.28	-0.44	... / 6 /	STV
233	17 00 00.62	-40 02 19.6	0.15	2.15	0.33	... / ... / 0
234	17 00 00.73	-40 08 47.8	0.19	0.24	-0.65	... / 2 / 0	0.32	...
235	17 00 02.54	-39 55 36.8	0.64	1.68	0.89	... / 1 / 0	0.80	...
236	17 00 02.58	-40 03 14.9	0.24	0.79	0.58	... / 0 / 1	0.08	...
237	17 00 03.18	-40 06 03.8	0.33	0.58	0.20	... / 0 / 0	1.00	...
238	17 00 03.37	-40 00 42.7	0.16	0.60	0.41	... / ... / 2
239	17 00 03.99	-40 01 11.0	0.20	0.56	0.74	... / 1 / 0	0.08	...
240	17 00 04.88	-40 07 20.1	0.29	0.28	-0.63	... / 2 / 0	0.49	...
241	17 00 06.63	-40 06 06.0	0.71	0.78	0.34	... / 2 / 0	3.24	LTV
242	17 00 06.83	-39 58 14.8	0.40	0.68	0.27	... / ... / 1
243	17 00 09.76	-40 10 30.7	0.25	0.40	-0.25	... / 0 /
244	17 00 10.46	-40 09 52.6	0.82	1.43	0.57	... / ... / 7	...	STV
245	17 00 13.72	-40 04 29.4	0.99	1.18	0.12	0 / 2 / 0	3.68	LTV
246	17 00 15.84	-40 07 10.7	1.38	1.60	-0.42	... / 9 /	STV
247	17 00 16.80	-40 06 47.4	0.95	2.39	0.76	... / 0 / 0	0.95	...
248	17 00 22.07	-40 03 59.6	1.09	2.65	0.79	... / 0 / 0	1.27	...
249	17 00 23.14	-40 05 22.2	2.00	4.37	0.90	... / 0 / 0	1.00	...

Table 3. X-Ray Properties

Source #	N_H 10^{22} cm^{-2}	kT (keV)	EM (cm $^{-3}$)	$F_{x,c}$ $10^{-14} \text{ (erg cm}^{-2} \text{ s}^{-1}\text{)}$	$\log L_{x,c}$ (erg s $^{-1}$)	reduced χ^2
(1)	(2)	(3)	(4)	(5)	(6)	(7)
3	1.07 $^{+0.28}_{-0.23}$	0.78	10.58 $^{+3.52}_{-2.93}$	11.93 $^{+3.42}_{-3.57}$	31.62	0.60
7	1.38 $^{+0.88}_{-0.58}$	1.23	3.09 $^{+2.21}_{-1.48}$	2.93 $^{+1.90}_{-1.72}$	31.01	0.64
8	0.42 $^{+0.42}_{-0.31}$	2.51 ^a	2.31 $^{+0.90}_{-0.72}$	2.45 $^{+0.84}_{-0.77}$	30.93	0.73
10	2.47 $^{+1.37}_{-0.89}$	2.52	3.18 $^{+1.48}_{-1.23}$	3.34 $^{+1.45}_{-1.46}$	31.06	0.74
12	3.81 $^{+1.78}_{-1.35}$	1.09	9.08 $^{+6.97}_{-5.09}$	9.30 $^{+6.25}_{-5.94}$	31.51	0.43
14	4.94 $^{+1.99}_{-1.37}$	1.88	14.68 $^{+6.36}_{-5.29}$	13.99 $^{+5.33}_{-5.63}$	31.68	0.51
15	1.08 $^{+0.95}_{-0.54}$	0.50 ^a	7.96 $^{+10.67}_{-5.12}$	7.91 $^{+5.93}_{-6.08}$	31.44	1.08
18	6.90 $^{+3.42}_{-2.02}$	1.87	10.16 $^{+5.31}_{-4.01}$	9.79 $^{+4.06}_{-4.55}$	31.53	0.95
20	0.42 $^{+0.40}_{-0.30}$	3.43	3.02 $^{+0.93}_{-0.81}$	3.68 $^{+1.07}_{-1.02}$	31.10	0.63
23	9.19 $^{+5.34}_{-4.57}$	0.50 ^a	262.64 $^{+849.34}_{-224.21}$	204.20 $^{+129.07}_{-172.07}$	32.85	0.60
24	1.71 $^{+1.40}_{-0.80}$	0.68	6.66 $^{+9.42}_{-4.78}$	7.70 $^{+7.14}_{-6.28}$	31.43	0.71
25	2.96 $^{+1.11}_{-0.80}$	5.47	9.50 $^{+2.59}_{-2.34}$	13.56 $^{+3.48}_{-3.93}$	31.67	0.87
26	1.32 $^{+0.36}_{-0.28}$	0.83	6.92 $^{+2.75}_{-2.22}$	7.81 $^{+3.10}_{-2.99}$	31.43	0.62
27	1.16 $^{+0.43}_{-0.33}$	1.28	5.48 $^{+2.04}_{-1.66}$	5.14 $^{+1.78}_{-1.77}$	31.25	0.69
29	1.66 $^{+0.65}_{-0.49}$	1.17	4.99 $^{+2.55}_{-1.98}$	5.45 $^{+2.05}_{-2.06}$	31.27	0.74
32	0.63 $^{+0.35}_{-0.30}$	1.32	3.22 $^{+1.50}_{-1.26}$	2.99 $^{+1.33}_{-1.29}$	31.01	0.80
34	0.80 $^{+0.36}_{-0.26}$	4.85 $^{+3.58}_{-1.74}$	13.37 $^{+4.78}_{-2.75}$	18.02 $^{+2.23}_{-2.52}$	31.79	0.86
35	0.28 $^{+0.20}_{-0.17}$	2.31	4.21 $^{+0.97}_{-0.85}$	4.28 $^{+0.90}_{-0.91}$	31.17	0.90
36	3.12 $^{+2.09}_{-1.29}$	1.18	10.73 $^{+9.41}_{-6.58}$	10.85 $^{+8.02}_{-7.66}$	31.57	0.76
37	1.12 $^{+0.31}_{-0.25}$	3.12	4.67 $^{+0.94}_{-0.88}$	5.44 $^{+1.04}_{-1.02}$	31.27	0.77
38	1.59 $^{+0.32}_{-0.26}$	1.29	13.10 $^{+3.31}_{-2.92}$	12.30 $^{+2.94}_{-2.83}$	31.63	0.81
39	1.22 $^{+1.19}_{-0.75}$	1.10 ^a	2.56 $^{+2.98}_{-1.80}$	2.67 $^{+2.35}_{-2.20}$	30.97	1.08
40	2.63 $^{+0.85}_{-0.65}$	2.01	12.83 $^{+4.05}_{-3.54}$	10.10 $^{+2.90}_{-2.75}$	31.54	0.77
41	0.96 $^{+0.86}_{-0.58}$	1.08	2.73 $^{+2.67}_{-1.71}$	5.39 $^{+5.65}_{-4.62}$	31.27	0.38
42	1.58 $^{+1.16}_{-0.68}$	0.86	3.21 $^{+3.75}_{-1.94}$	3.59 $^{+3.13}_{-2.52}$	31.09	0.69
44	2.63 $^{+1.87}_{-1.08}$	2.43	2.16 $^{+1.34}_{-1.05}$	2.23 $^{+1.39}_{-1.34}$	30.89	0.33
45	1.28 $^{+0.97}_{-0.58}$	1.79	3.76 $^{+2.31}_{-1.78}$	3.48 $^{+1.88}_{-1.87}$	31.08	0.78
46	2.95 $^{+1.01}_{-0.77}$	2.16	9.01 $^{+2.94}_{-2.58}$	8.91 $^{+2.76}_{-2.97}$	31.49	0.61
48	1.79 $^{+0.81}_{-0.57}$	6.75	2.98 $^{+0.88}_{-0.80}$	4.41 $^{+1.27}_{-1.32}$	31.18	0.74
49	2.04 $^{+0.63}_{-0.60}$	0.94 $^{+0.53}_{-0.28}$	12.55 $^{+17.16}_{-7.17}$	13.86 $^{+8.43}_{-8.77}$	31.68	0.68
51	1.50 $^{+1.29}_{-0.77}$	0.79	2.97 $^{+3.90}_{-2.16}$	3.47 $^{+3.26}_{-2.79}$	31.08	0.30
52	2.31 $^{+2.31}_{-1.13}$	0.87	6.02 $^{+9.33}_{-4.13}$	7.09 $^{+6.98}_{-5.75}$	31.39	0.75
54	1.06 $^{+0.66}_{-0.40}$	0.96	2.20 $^{+1.65}_{-1.03}$	2.42 $^{+1.33}_{-1.42}$	30.92	1.09
55	1.72 $^{+1.85}_{-1.09}$	0.86	7.96 $^{+13.25}_{-6.20}$	9.87 $^{+11.53}_{-8.03}$	31.53	1.06
58	2.16 $^{+1.24}_{-0.77}$	3.43	3.98 $^{+1.60}_{-1.34}$	4.87 $^{+1.69}_{-1.84}$	31.23	0.71
59	2.16 $^{+2.32}_{-1.13}$	2.90	1.11 $^{+0.85}_{-0.63}$	1.28 $^{+0.81}_{-0.79}$	30.65	0.24
63	7.15 $^{+2.59}_{-1.78}$	3.06 $^{+2.65}_{-1.10}$	34.01 $^{+39.73}_{-15.74}$	38.79 $^{+16.36}_{-26.17}$	32.13	0.60
65	4.54 $^{+2.22}_{-1.66}$	1.73	7.94 $^{+4.17}_{-3.43}$	7.33 $^{+3.36}_{-3.72}$	31.40	0.85
71	2.00 $^{+0.84}_{-0.64}$	2.16	4.94 $^{+1.96}_{-1.63}$	4.90 $^{+1.73}_{-1.87}$	31.23	0.78
72	1.56 $^{+1.12}_{-0.71}$	1.72	1.49 $^{+1.01}_{-0.77}$	1.34 $^{+0.82}_{-0.76}$	30.67	0.58
73	1.56 $^{+1.37}_{-0.82}$	3.08	1.48 $^{+1.00}_{-0.73}$	1.69 $^{+1.01}_{-0.96}$	30.77	0.53
88	1.71 $^{+1.46}_{-0.82}$	1.10	2.21 $^{+2.30}_{-1.34}$	2.18 $^{+1.77}_{-1.53}$	30.88	0.69
89	4.68 $^{+1.84}_{-1.26}$	3.19	9.43 $^{+3.18}_{-2.74}$	10.93 $^{+3.61}_{-3.59}$	31.58	1.15
95	4.12 $^{+3.45}_{-2.08}$	0.55	53.71 $^{+142.36}_{-43.67}$	61.72 $^{+73.66}_{-54.22}$	32.33	0.26

Table 3 continued on next page

Table 3 (*continued*)

Source #	N_H 10^{22} (cm $^{-2}$)	kT (keV)	EM (cm $^{-3}$)	$F_{x,c}$ 10^{-14} (erg cm $^{-2}$ s $^{-1}$)	$\log L_{x,c}$ (erg s $^{-1}$)	reduced χ^2
(1)	(2)	(3)	(4)	(5)	(6)	(7)
102	4.80 $^{+1.68}_{-1.10}$	1.96	14.76 $^{+5.33}_{-4.32}$	14.13 $^{+4.99}_{-4.74}$	31.69	0.67
103	5.22 $^{+1.23}_{-0.87}$	8.62	12.81 $^{+2.24}_{-2.00}$	19.83 $^{+3.37}_{-3.35}$	31.84	0.60
104	26.12 $^{+26.31}_{-11.88}$	2.23	16.58 $^{+26.46}_{-10.83}$	17.43 $^{+13.88}_{-13.98}$	31.78	0.54
108	1.61 $^{+1.00}_{-0.61}$	2.70	1.41 $^{+0.66}_{-0.55}$	1.58 $^{+0.63}_{-0.67}$	30.74	0.52
111	1.63 $^{+0.84}_{-0.56}$	3.38	1.97 $^{+0.73}_{-0.64}$	2.36 $^{+0.90}_{-0.83}$	30.91	0.54
112	3.44 $^{+1.73}_{-1.12}$	1.37	3.37 $^{+2.10}_{-1.65}$	2.98 $^{+1.89}_{-1.67}$	31.01	0.63
114	1.92 $^{+1.71}_{-1.00}$	1.86	2.44 $^{+1.92}_{-1.31}$	2.30 $^{+1.57}_{-1.49}$	30.90	0.77
115	1.79 $^{+1.32}_{-0.89}$	1.69	2.16 $^{+1.59}_{-1.16}$	2.05 $^{+1.24}_{-1.32}$	30.85	0.51
116	1.33 $^{+1.11}_{-0.62}$	7.72	1.52 $^{+0.65}_{-0.57}$	2.34 $^{+0.85}_{-0.91}$	30.91	0.41
120	2.43 $^{+1.00}_{-0.75}$	1.72	4.11 $^{+1.83}_{-1.56}$	3.77 $^{+1.65}_{-1.64}$	31.12	0.55
121	2.05 $^{+0.58}_{-0.40}$	3.00 $^{+1.20}_{-0.89}$	24.70 $^{+13.36}_{-6.68}$	28.13 $^{+5.16}_{-8.29}$	31.99	0.80
127	1.38 $^{+1.18}_{-0.64}$	1.20	2.32 $^{+2.31}_{-1.26}$	2.23 $^{+1.57}_{-1.58}$	30.89	0.69
129	1.84 $^{+0.94}_{-0.65}$	4.60	2.17 $^{+0.74}_{-0.65}$	2.94 $^{+0.95}_{-1.06}$	31.01	0.51
130	1.52 $^{+1.16}_{-0.70}$	2.98	1.42 $^{+0.77}_{-0.61}$	1.62 $^{+0.75}_{-0.81}$	30.75	0.48
131	1.15 $^{+0.33}_{-0.26}$	1.34	6.07 $^{+1.84}_{-1.58}$	5.73 $^{+1.54}_{-1.65}$	31.30	0.57
137	5.08 $^{+5.03}_{-2.20}$	2.95	3.72 $^{+2.91}_{-1.74}$	4.16 $^{+2.68}_{-2.43}$	31.16	0.41
138	6.55 $^{+2.71}_{-1.75}$	1.12	19.99 $^{+12.48}_{-9.25}$	20.37 $^{+10.37}_{-10.88}$	31.85	0.64
139	0.66 $^{+0.27}_{-0.23}$	0.99	3.01 $^{+1.36}_{-1.12}$	3.29 $^{+1.22}_{-1.44}$	31.06	0.53
143	3.19 $^{+1.35}_{-0.92}$	2.93	3.41 $^{+1.25}_{-1.09}$	3.89 $^{+1.18}_{-1.32}$	31.13	0.67
144	2.12 $^{+1.24}_{-0.72}$	4.83	1.47 $^{+0.58}_{-0.50}$	2.02 $^{+0.71}_{-0.76}$	30.84	0.50
146	1.29 $^{+0.33}_{-0.24}$	0.74	8.70 $^{+3.47}_{-2.74}$	9.82 $^{+3.11}_{-3.50}$	31.53	0.78
149	3.86 $^{+1.41}_{-0.95}$	0.73	16.34 $^{+11.28}_{-7.61}$	18.19 $^{+10.38}_{-10.33}$	31.80	0.59
150	1.88 $^{+1.37}_{-0.78}$	1.23	6.17 $^{+4.80}_{-3.20}$	6.00 $^{+3.88}_{-3.81}$	31.32	0.79
151	4.62 $^{+1.07}_{-0.83}$	1.86	11.68 $^{+3.23}_{-2.91}$	11.07 $^{+2.91}_{-2.95}$	31.58	0.86
154	14.37 $^{+9.47}_{-4.92}$	1.19	24.07 $^{+24.32}_{-13.60}$	24.21 $^{+16.24}_{-16.74}$	31.92	0.31
155	14.75 $^{+4.46}_{-3.31}$	1.98	25.99 $^{+10.54}_{-8.45}$	24.97 $^{+9.85}_{-10.00}$	31.94	0.60
157	16.36 $^{+5.22}_{-6.17}$	0.68	138.65 $^{+237.17}_{-102.25}$	93.63 $^{+54.43}_{-81.50}$	32.51	0.12
168	3.49 $^{+0.89}_{-0.70}$	1.87 $^{+0.67}_{-0.42}$	22.59 $^{+15.33}_{-8.62}$	21.02 $^{+10.72}_{-9.59}$	31.86	0.60
170	15.25 $^{+9.16}_{-5.36}$	4.22	5.86 $^{+4.03}_{-2.65}$	7.64 $^{+4.12}_{-4.21}$	31.42	0.35
171	15.18 $^{+7.80}_{-4.67}$	0.69	133.86 $^{+158.73}_{-84.23}$	149.45 $^{+124.59}_{-109.70}$	32.71	0.17
172	1.71 $^{+0.62}_{-0.45}$	0.29	55.09 $^{+51.18}_{-29.15}$	31.04 $^{+22.15}_{-19.40}$	32.03	0.43
174	5.40 $^{+5.23}_{-2.33}$	3.37	1.72 $^{+1.19}_{-0.87}$	2.10 $^{+1.10}_{-1.18}$	30.86	0.26
178	41.35 $^{+30.19}_{-14.84}$	4.06	15.90 $^{+20.40}_{-8.51}$	20.80 $^{+15.81}_{-14.39}$	31.86	0.90
181	1.97 $^{+1.82}_{-1.02}$	1.92	1.99 $^{+1.56}_{-1.15}$	1.82 $^{+1.32}_{-1.27}$	30.80	0.05
187	5.07 $^{+1.91}_{-1.55}$	0.68	54.62 $^{+44.81}_{-31.75}$	61.49 $^{+43.73}_{-42.42}$	32.33	0.25
189	19.61 $^{+10.11}_{-5.94}$	5.30	16.05 $^{+9.11}_{-6.03}$	22.72 $^{+10.00}_{-9.85}$	31.90	0.41
191	4.44 $^{+3.20}_{-1.59}$	1.94	3.16 $^{+2.15}_{-1.56}$	3.06 $^{+1.65}_{-1.72}$	31.02	0.46
192	6.11 $^{+1.27}_{-1.11}$	0.54	212.07 $^{+115.26}_{-86.53}$	213.62 $^{+98.16}_{-107.67}$	32.87	0.61
195	3.06 $^{+2.56}_{-1.61}$	0.50	19.93 $^{+37.14}_{-16.49}$	19.97 $^{+20.53}_{-16.24}$	31.84	0.77
202	3.04 $^{+1.69}_{-1.16}$	2.45	3.06 $^{+1.54}_{-1.26}$	3.66 $^{+1.86}_{-1.87}$	31.10	0.72
205	4.26 $^{+1.66}_{-1.17}$	0.89	16.52 $^{+10.72}_{-7.65}$	18.20 $^{+9.76}_{-10.28}$	31.80	0.48
206	5.86 $^{+1.95}_{-3.00}$	0.43	107.37 $^{+252.53}_{-94.25}$	46.43 $^{+36.49}_{-40.67}$	32.21	0.01
209	4.84 $^{+1.88}_{-1.30}$	2.03	6.67 $^{+2.74}_{-2.29}$	6.50 $^{+2.43}_{-2.52}$	31.35	0.66
212	2.17 $^{+1.14}_{-0.87}$	1.43 $^{+0.85}_{-0.52}$	7.34 $^{+13.28}_{-4.04}$	7.09 $^{+7.57}_{-5.60}$	31.39	0.56
213	4.04 $^{+1.42}_{-1.02}$	1.95	6.46 $^{+2.38}_{-2.04}$	6.22 $^{+2.22}_{-2.08}$	31.33	0.77
216	0.64 $^{+0.44}_{-0.33}$	3.73	1.47 $^{+0.51}_{-0.45}$	1.83 $^{+0.59}_{-0.61}$	30.80	0.71

Table 3 continued on next page

Table 3 (*continued*)

Source #	N_H 10^{22} (cm $^{-2}$)	kT (keV)	EM (cm $^{-3}$)	$F_{x,c}$ 10^{-14} (erg cm $^{-2}$ s $^{-1}$)	$\log L_{x,c}$ (erg s $^{-1}$)	reduced χ^2
(1)	(2)	(3)	(4)	(5)	(6)	(7)
221	0.21 $^{+0.22}_{-0.20}$	0.68	0.98 $^{+0.58}_{-0.45}$	1.12 $^{+0.59}_{-0.55}$	30.59	0.51
225	3.41 $^{+2.15}_{-1.36}$	0.86	7.64 $^{+8.32}_{-4.99}$	8.77 $^{+7.47}_{-6.80}$	31.48	0.47
228	1.47 $^{+1.02}_{-0.71}$	2.65	2.89 $^{+1.42}_{-1.16}$	3.09 $^{+1.44}_{-1.37}$	31.03	1.08
230	10.43 $^{+5.83}_{-3.49}$	5.44	6.28 $^{+2.97}_{-2.15}$	9.06 $^{+3.44}_{-3.66}$	31.50	0.65
235	24.92 $^{+11.69}_{-7.43}$	1.12	168.06 $^{+152.19}_{-83.18}$	169.98 $^{+112.16}_{-106.21}$	32.77	0.53
241	4.37 $^{+1.37}_{-1.09}$	0.89	18.60 $^{+10.32}_{-7.98}$	21.03 $^{+10.69}_{-10.12}$	31.86	0.57
244	5.26 $^{+3.83}_{-1.93}$	1.64	10.93 $^{+8.37}_{-5.50}$	10.10 $^{+6.05}_{-6.41}$	31.54	0.53
245	1.63 $^{+0.65}_{-0.50}$	1.78	3.91 $^{+1.48}_{-1.27}$	3.63 $^{+1.27}_{-1.34}$	31.10	0.58

Table 4. Infrared Counterparts

Source #	J	H	K _S	[3.6]	[4.5]	[5.8]	[8.0]	Type
(1)	(2)	(3)	(4)	(5)	(6)	(7)	(8)	(9)
1	Galactic contamination
2	...	17.58 ± 0.09	16.99 ± 0.09	Class III
3	12.877 ± 0.001	12.166 ± 0.001	12.040 ± 0.001	11.71 ± 0.05	11.65 ± 0.07	11.51 ± 0.09	...	Contamination
4	17.61 ± 0.16
5	14.244 ± 0.003	13.584 ± 0.003	13.324 ± 0.004	13.03 ± 0.07	13.32 ± 0.11	Contamination
6	AGN
7	Class II
8	11.774 ± 0.001	11.436 ± 0.001	10.601 ± 0.001	10.56 ± 0.09	10.40 ± 0.10	10.16 ± 0.06	9.98 ± 0.06	Contamination
9	14.942 ± 0.004	14.049 ± 0.004	13.670 ± 0.005	13.20 ± 0.07	13.22 ± 0.10	Class III
10	...	16.38 ± 0.03	14.13 ± 0.01	12.23 ± 0.08	11.69 ± 0.09	Field Star
11	18.73 ± 0.11	17.67 ± 0.10
12	16.60 ± 0.02	14.043 ± 0.004	12.369 ± 0.002	10.89 ± 0.04	10.15 ± 0.05	9.50 ± 0.06	9.10 ± 0.12	Class II
13	AGN
14	15.11 ± 0.01	13.052 ± 0.002	11.608 ± 0.001	9.79 ± 0.04	8.87 ± 0.04	8.10 ± 0.03	7.16 ± 0.02	Class II
15	14.713 ± 0.004	13.841 ± 0.003	13.385 ± 0.004	13.01 ± 0.06	13.04 ± 0.12	Class III
16	19.13 ± 0.15	17.54 ± 0.08	16.86 ± 0.08	Class III
17	14.861 ± 0.004	13.721 ± 0.003	13.038 ± 0.003	12.29 ± 0.04	11.88 ± 0.07	11.53 ± 0.27	...	Class III
18	18.08 ± 0.25
19	17.76 ± 0.19
20	14.650 ± 0.004	13.342 ± 0.002	12.311 ± 0.002	11.42 ± 0.16	11.35 ± 0.17	Class II
21	16.07 ± 0.01	14.55 ± 0.01	13.519 ± 0.004	12.40 ± 0.08	11.90 ± 0.11	Class II
22	12.871 ± 0.001	12.072 ± 0.001	10.896 ± 0.001	9.41 ± 0.04	8.95 ± 0.04	8.57 ± 0.05	7.84 ± 0.08	Class I
23	16.96 ± 0.02	16.58 ± 0.04	Contamination
24	11.513 ± 0.001	10.123 ± 0.001	9.322 ± 0.001	9.12 ± 0.10	8.95 ± 0.13	8.32 ± 0.07	6.96 ± 0.20	Class III
25	16.43 ± 0.01	14.81 ± 0.01	13.80 ± 0.01	12.99 ± 0.05	12.55 ± 0.08	12.07 ± 0.32	...	Class II
26	13.339 ± 0.002	...	12.139 ± 0.002	11.77 ± 0.07	11.76 ± 0.16	Field Star
27	13.129 ± 0.001	12.346 ± 0.001	11.932 ± 0.001	11.66 ± 0.06	11.60 ± 0.10	Class III
28	15.062 ± 0.005	13.498 ± 0.003	12.636 ± 0.002	12.03 ± 0.07	12.04 ± 0.10	Class III
29	12.454 ± 0.001	11.509 ± 0.001	10.533 ± 0.001	8.98 ± 0.05	8.37 ± 0.05	7.83 ± 0.03	7.32 ± 0.04	Class II
30	14.148 ± 0.003	13.114 ± 0.002	12.329 ± 0.002	11.43 ± 0.04	10.95 ± 0.05	10.68 ± 0.07	...	Class II
31	AGN
32	13.940 ± 0.002	...	12.518 ± 0.002	Class II
33	...	19.21 ± 0.39	18.48 ± 0.37
34	...	15.01 ± 0.01

Table 4 continued on next page

Table 4 (*continued*)

Source #	J	H	K _S	[3.6]	[4.5]	[5.8]	[8.0]	Type
(1)	(2)	(3)	(4)	(5)	(6)	(7)	(8)	(9)
35	11.112 ± 0.001	12.378 ± 0.001	10.204 ± 0.001	9.84 ± 0.04	9.88 ± 0.05	9.82 ± 0.05	9.90 ± 0.08	Contamination
36	15.52 ± 0.01	14.58 ± 0.01	14.16 ± 0.01	13.98 ± 0.10	14.06 ± 0.36	Class III
37	13.509 ± 0.002	12.051 ± 0.001	11.824 ± 0.001	10.75 ± 0.04	10.49 ± 0.05	10.19 ± 0.06	10.17 ± 0.08	Contamination
38	13.242 ± 0.002	12.661 ± 0.001	11.968 ± 0.001	11.73 ± 0.06	11.49 ± 0.08	11.31 ± 0.09	...	Contamination
39	...	17.41 ± 0.08	16.55 ± 0.06	Class III
40	...	9.555 ± 0.001	...	8.53 ± 0.05	8.48 ± 0.12	8.38 ± 0.24	...	Field Star
41	14.418 ± 0.003	13.388 ± 0.002	12.721 ± 0.002	11.22 ± 0.10	10.76 ± 0.10	Class II
42	14.564 ± 0.003	13.392 ± 0.002	12.824 ± 0.003	12.16 ± 0.09	11.93 ± 0.11	Class III
43	13.679 ± 0.002	12.634 ± 0.001	11.675 ± 0.001	Class II
44	15.80 ± 0.01	14.96 ± 0.01	14.54 ± 0.01	Class III
45	16.49 ± 0.01	15.27 ± 0.01	14.55 ± 0.01	14.03 ± 0.10	13.63 ± 0.13	Class III
46	18.47 ± 0.09	15.80 ± 0.02	14.45 ± 0.01	13.13 ± 0.12	12.63 ± 0.34	Class III
47	16.52 ± 0.02	15.58 ± 0.01	15.05 ± 0.02	Class III
48	15.70 ± 0.01	14.115 ± 0.004	13.031 ± 0.003	11.80 ± 0.05	11.33 ± 0.06	10.94 ± 0.10	...	Class II
49	14.467 ± 0.003	13.329 ± 0.002	12.771 ± 0.002	12.39 ± 0.04	12.18 ± 0.07	12.10 ± 0.13	...	Class III
50	15.94 ± 0.01	14.86 ± 0.01	14.27 ± 0.01	13.79 ± 0.06	13.72 ± 0.14	Class III
51	17.42 ± 0.03	16.45 ± 0.03	15.92 ± 0.03	Class III
52	15.12 ± 0.01	13.600 ± 0.003	12.820 ± 0.003	12.57 ± 0.14	12.30 ± 0.10	Class III
53	14.77 ± 0.01	11.28 ± 0.08	10.47 ± 0.10	9.30 ± 0.12	9.03 ± 0.22	Field Star
54	14.019 ± 0.002	13.052 ± 0.002	12.610 ± 0.002	12.35 ± 0.05	12.25 ± 0.08	12.13 ± 0.16	...	Class III
55	15.24 ± 0.01	14.080 ± 0.004	13.409 ± 0.004	12.50 ± 0.05	12.22 ± 0.07	11.55 ± 0.15	...	Class III
56	13.238 ± 0.002	12.670 ± 0.001	12.350 ± 0.002	12.10 ± 0.06	12.00 ± 0.08	Contamination
57	15.56 ± 0.01	14.302 ± 0.005	13.626 ± 0.005	12.44 ± 0.07	11.90 ± 0.07	11.22 ± 0.09	10.78 ± 0.19	Class III
58
59
60	Class II
61	16.99 ± 0.02	15.43 ± 0.01	13.487 ± 0.004	10.63 ± 0.08	9.53 ± 0.07	8.67 ± 0.07	...	Class I
62	14.103 ± 0.003	13.048 ± 0.002	12.568 ± 0.002	11.72 ± 0.06	11.39 ± 0.08	Class III
63	16.27 ± 0.01	14.46 ± 0.01	13.248 ± 0.003	11.19 ± 0.15	10.63 ± 0.21	Class II
64	15.33 ± 0.01	14.119 ± 0.004	13.558 ± 0.005	12.95 ± 0.17	12.80 ± 0.18	Class III
65
66	18.96 ± 0.13	17.26 ± 0.07	16.58 ± 0.06	Class III
67	14.930 ± 0.004	13.725 ± 0.003	12.80 ± 0.00	11.57 ± 0.04	11.17 ± 0.06	10.76 ± 0.07	10.12 ± 0.07	Class II
68	15.73 ± 0.01	14.73 ± 0.01	14.30 ± 0.01	14.05 ± 0.09	Class III
69
70	AGN

Table 4 (*continued* on next page)

Table 4 (continued)

Source #	J	H	K _S	[3.6]	[4.5]	[5.8]	[8.0]	Type
(1)	(2)	(3)	(4)	(5)	(6)	(7)	(8)	(9)
71	16.45 ± 0.01	14.110 ± 0.004	12.803 ± 0.002	10.98 ± 0.07	10.89 ± 0.08	10.35 ± 0.13	...	Class III
72	14.917 ± 0.004	13.581 ± 0.003	12.567 ± 0.002	11.25 ± 0.05	10.73 ± 0.05	10.20 ± 0.07	...	Class II
73	14.456 ± 0.003	13.585 ± 0.003	13.183 ± 0.003	12.78 ± 0.05	12.66 ± 0.09	Class III
74	AGN
75	16.29 ± 0.01	15.31 ± 0.01	14.81 ± 0.01	Class III
76	14.504 ± 0.003	12.679 ± 0.001	11.269 ± 0.001	9.83 ± 0.04	9.32 ± 0.05	8.85 ± 0.07	7.99 ± 0.09	Class I
77	15.57 ± 0.01	14.90 ± 0.01	14.53 ± 0.01	13.91 ± 0.10	14.03 ± 0.20	Class III
78	14.891 ± 0.004	13.607 ± 0.003	13.001 ± 0.003	12.50 ± 0.08	12.35 ± 0.13	11.20 ± 0.35	...	Class III
79	14.054 ± 0.003	13.197 ± 0.002	12.533 ± 0.002	12.31 ± 0.05	12.14 ± 0.07	11.96 ± 0.11	...	Class II
80	...	17.83 ± 0.11	17.07 ± 0.10	Class III
81	14.506 ± 0.003	13.249 ± 0.002	12.478 ± 0.002	11.30 ± 0.04	11.04 ± 0.06	10.61 ± 0.08	9.64 ± 0.13	Class III
82
83	...	16.23 ± 0.03	13.95 ± 0.01	11.15 ± 0.04	10.05 ± 0.05	9.23 ± 0.04	8.57 ± 0.03	Field Star
84	...	17.53 ± 0.08	16.78 ± 0.08	Class III
85	15.20 ± 0.01	14.106 ± 0.004	13.578 ± 0.005	13.08 ± 0.10	13.11 ± 0.11	Class III
86	Class II
87
88	15.054 ± 0.005	13.859 ± 0.003	13.318 ± 0.004	12.88 ± 0.06	12.85 ± 0.11	Class III
89	19.55 ± 0.23	16.24 ± 0.03	14.25 ± 0.01	Class II
90	19.30 ± 0.18	16.12 ± 0.02	14.19 ± 0.01	12.22 ± 0.11	11.43 ± 0.19	Class II
91	18.04 ± 0.06	15.76 ± 0.02	14.61 ± 0.01	13.85 ± 0.12	13.56 ± 0.16	Class III
92	15.22 ± 0.01	14.207 ± 0.004	13.72 ± 0.01	13.36 ± 0.07	13.21 ± 0.13	Class III
93	16.38 ± 0.01	14.89 ± 0.01	14.16 ± 0.01	13.42 ± 0.10	12.90 ± 0.14	Class III
94
95	14.21 ± 0.11	13.86 ± 0.18	...	Class II
96	16.31 ± 0.01	15.57 ± 0.01	15.20 ± 0.02	Class III
97	16.65 ± 0.02	14.62 ± 0.01	13.571 ± 0.005	12.90 ± 0.07	12.79 ± 0.10	Class III
98	18.03 ± 0.06	16.58 ± 0.04	15.93 ± 0.04	Class III
99	16.79 ± 0.02	14.75 ± 0.01	13.594 ± 0.005	12.19 ± 0.24	11.40 ± 0.21	Class III
100	...	17.48 ± 0.08	15.71 ± 0.03	Class II
101	16.01 ± 0.01	14.45 ± 0.01	13.601 ± 0.005	12.73 ± 0.07	12.71 ± 0.12	Class III
102	15.16 ± 0.01	11.85 ± 0.00	10.454 ± 0.001	Contamination
103	...	17.30 ± 0.07	13.386 ± 0.004	10.34 ± 0.05	8.88 ± 0.08	8.01 ± 0.03	7.28 ± 0.07	Field Star
104	19.13 ± 0.15	17.00 ± 0.05	15.86 ± 0.03	Class III
105	...	14.020 ± 0.004	13.486 ± 0.004	12.00 ± 0.06	11.88 ± 0.08	11.65 ± 0.09	...	Field Star
106	15.91 ± 0.01	...	13.83 ± 0.01	13.21 ± 0.09	13.22 ± 0.20	Field Star

Table 4 continued on next page

Table 4 (*continued*)

Source #	J	H	K _S	[3.6]	[4.5]	[5.8]	[8.0]	Type
(1)	(2)	(3)	(4)	(5)	(6)	(7)	(8)	(9)
107	17.83 ± 0.20
108	15.74 ± 0.01	14.222 ± 0.004	13.461 ± 0.004	12.81 ± 0.05	12.62 ± 0.11	Class III
109	16.54 ± 0.02	14.89 ± 0.01	13.79 ± 0.01	12.15 ± 0.05	11.66 ± 0.08	11.03 ± 0.08	9.96 ± 0.09	Class II
110	17.64 ± 0.04	15.93 ± 0.02	14.99 ± 0.02	14.29 ± 0.14	14.00 ± 0.22	Class III
111	16.45 ± 0.01	14.330 ± 0.005	13.241 ± 0.003	12.52 ± 0.06	12.41 ± 0.08	Class III
112	16.06 ± 0.01	14.306 ± 0.005	13.420 ± 0.004	12.59 ± 0.07	12.58 ± 0.12	Class III
113	17.46 ± 0.03	15.80 ± 0.02	14.99 ± 0.02	Class III
114
115	17.32 ± 0.03	16.07 ± 0.02	15.40 ± 0.02	Class III
116	14.980 ± 0.005	13.168 ± 0.002	12.236 ± 0.002	11.45 ± 0.07	11.27 ± 0.10	Class III
117
118	15.65 ± 0.03
119	16.43 ± 0.01	14.85 ± 0.01	13.83 ± 0.01	12.61 ± 0.09	12.29 ± 0.21	11.16 ± 0.17	...	Class II
120	15.087 ± 0.005	13.564 ± 0.003	12.816 ± 0.003	12.41 ± 0.09	12.26 ± 0.20	Class III
121	12.051 ± 0.001	12.185 ± 0.001	9.984 ± 0.001	9.49 ± 0.03	9.34 ± 0.05	9.19 ± 0.04	9.12 ± 0.05	Contamination
122	15.017 ± 0.005	13.397 ± 0.002	12.129 ± 0.002	10.64 ± 0.04	10.12 ± 0.05	9.79 ± 0.05	9.39 ± 0.06	Class II
123	16.21 ± 0.01	14.89 ± 0.01	14.00 ± 0.01	13.50 ± 0.20	Class II
124	18.49 ± 0.09	17.41 ± 0.07	16.82 ± 0.08	Class III
125	15.99 ± 0.01	14.62 ± 0.01	13.83 ± 0.01	13.17 ± 0.12	Class III
126	17.00 ± 0.02	15.37 ± 0.01	14.42 ± 0.01	13.54 ± 0.12	13.38 ± 0.24	Class II
127	15.87 ± 0.01	14.41 ± 0.01	13.67 ± 0.01	12.61 ± 0.07	12.38 ± 0.10	Class III
128
129	15.93 ± 0.01	14.224 ± 0.004	13.378 ± 0.004	12.47 ± 0.07	12.10 ± 0.07	Class III
130	15.71 ± 0.01	14.165 ± 0.004	13.371 ± 0.004	12.83 ± 0.05	12.64 ± 0.08	Class III
131	11.492 ± 0.001	10.808 ± 0.001	10.406 ± 0.001	10.14 ± 0.06	10.12 ± 0.08	9.82 ± 0.11	...	Class III
132	13.376 ± 0.002	13.053 ± 0.002	12.759 ± 0.002	12.58 ± 0.14	12.40 ± 0.32	Contamination
133	14.712 ± 0.004	13.033 ± 0.002	11.607 ± 0.001	9.90 ± 0.04	9.17 ± 0.04	8.69 ± 0.06	7.98 ± 0.09	Class I
134	15.60 ± 0.01	14.128 ± 0.004	13.361 ± 0.004	Class III
135	15.83 ± 0.01	14.50 ± 0.01	13.489 ± 0.004	12.53 ± 0.09	12.09 ± 0.10	Class II
136	11.742 ± 0.001	12.172 ± 0.001	10.724 ± 0.001	8.82 ± 0.10	8.54 ± 0.29	8.22 ± 0.30	...	Contamination
137	17.73 ± 0.04	14.57 ± 0.01	12.738 ± 0.002	10.71 ± 0.04	10.06 ± 0.06	9.44 ± 0.06	9.38 ± 0.24	Class II
138	19.05 ± 0.15	15.36 ± 0.01	13.297 ± 0.004	12.09 ± 0.07	11.64 ± 0.09	11.12 ± 0.13	...	Class II
139	...	10.383 ± 0.001	...	7.69 ± 0.03	7.60 ± 0.04	7.52 ± 0.03	7.58 ± 0.06	Field Star
140	19.06 ± 0.15	16.30 ± 0.03
141	16.57 ± 0.02	13.677 ± 0.003	11.882 ± 0.001	9.49 ± 0.05	8.66 ± 0.05	7.91 ± 0.04	7.12 ± 0.05	Class III
142	18.84 ± 0.12	16.16 ± 0.02	14.56 ± 0.01	12.95 ± 0.06	12.23 ± 0.07	11.51 ± 0.11	...	Class II

Table 4 *continued on next page*

Table 4 (*continued*)

Source #	J	H	K _S	[3.6]	[4.5]	[5.8]	[8.0]	Type
(1)	(2)	(3)	(4)	(5)	(6)	(7)	(8)	(9)
143	...	14.84 ± 0.01	13.257 ± 0.004	Class II
144	15.42 ± 0.01	13.462 ± 0.002	12.163 ± 0.002	10.50 ± 0.04	10.02 ± 0.06	9.61 ± 0.04	9.09 ± 0.07	Class II
145	16.86 ± 0.02	14.212 ± 0.004	12.760 ± 0.003	11.39 ± 0.05	10.89 ± 0.06	10.60 ± 0.12	9.85 ± 0.10	Class III
146	9.188 ± 0.001	8.725 ± 0.001	9.730 ± 0.001	7.05 ± 0.04	6.78 ± 0.04	6.56 ± 0.03	...	Contamination
147	19.45 ± 0.21	15.92 ± 0.02	14.21 ± 0.01	13.12 ± 0.08	Class III
148	16.10 ± 0.01	14.85 ± 0.01	14.20 ± 0.01	13.66 ± 0.09	13.42 ± 0.20	Class III
149	15.47 ± 0.01	13.597 ± 0.003	12.357 ± 0.002	10.99 ± 0.04	10.61 ± 0.05	10.17 ± 0.06	9.94 ± 0.10	Class II
150	14.366 ± 0.003	13.270 ± 0.002	12.717 ± 0.002	12.49 ± 0.06	12.31 ± 0.09	Class III
151	18.92 ± 0.13	15.44 ± 0.01	13.364 ± 0.004	12.12 ± 0.07	11.69 ± 0.09	11.54 ± 0.18	...	Class II
152	...	18.00 ± 0.13	...	12.01 ± 0.10	11.13 ± 0.09	10.79 ± 0.10	...	Field Star
153	...	14.73 ± 0.01	13.68 ± 0.01	12.97 ± 0.15	Field Star
154	18.95 ± 0.13	15.36 ± 0.01	13.146 ± 0.003	Class II
155
156	19.69 ± 0.26	15.69 ± 0.02	13.288 ± 0.004	Class II
157	17.50 ± 0.04	15.67 ± 0.02	14.57 ± 0.01	13.17 ± 0.08	12.51 ± 0.11	Class II
158	16.16 ± 0.01	14.76 ± 0.01	14.04 ± 0.01	13.41 ± 0.10	13.26 ± 0.14	Class III
159	14.829 ± 0.004	14.298 ± 0.005	13.96 ± 0.01	Contamination
160	13.92 ± 0.01
161	12.123 ± 0.002	High-mass protostar
162
163
164	15.45 ± 0.01	13.627 ± 0.003	12.617 ± 0.002	11.32 ± 0.13	10.65 ± 0.31	10.00 ± 0.17	...	Class III
165	17.31 ± 0.03	16.63 ± 0.04	16.19 ± 0.05	Class III
166	17.47 ± 0.04	15.03 ± 0.01
167	14.52 ± 0.01	11.35 ± 0.05	10.07 ± 0.04	9.19 ± 0.04	8.39 ± 0.03	Field Star
168	13.968 ± 0.002	12.491 ± 0.001	10.502 ± 0.001	9.42 ± 0.04	9.18 ± 0.05	9.08 ± 0.06	...	Class I
169
170
171	17.48 ± 0.04	15.28 ± 0.01	14.01 ± 0.01	Class II
172	11.555 ± 0.001	12.366 ± 0.001	8.732 ± 0.001	8.24 ± 0.04	8.16 ± 0.04	8.12 ± 0.04	8.25 ± 0.11	Contamination
173	17.41 ± 0.03	15.36 ± 0.01	14.14 ± 0.01	12.61 ± 0.05	12.11 ± 0.09	11.55 ± 0.10	...	Class II
174
175	18.66 ± 0.10	16.12 ± 0.02	14.68 ± 0.01	13.37 ± 0.08	12.70 ± 0.11	Class II
176	15.52 ± 0.01	14.157 ± 0.005	13.467 ± 0.004	Class III
177
178

Table 4 continued on next page

Table 4 (continued)

Source #	J	H	K _S	[3.6]	[4.5]	[5.8]	[8.0]	Type
(1)	(2)	(3)	(4)	(5)	(6)	(7)	(8)	(9)
179
180	17.75 ± 0.05	14.56 ± 0.01	12.626 ± 0.002	10.72 ± 0.04	9.89 ± 0.07	9.33 ± 0.05	8.93 ± 0.07	Class III
181	17.35 ± 0.03	16.14 ± 0.02	15.39 ± 0.02	Class III
182	...	16.53 ± 0.03	14.01 ± 0.01	Class II
183	13.082 ± 0.001	12.456 ± 0.001	12.333 ± 0.002	12.56 ± 0.15	Contamination
184	17.14 ± 0.03	15.28 ± 0.01	14.07 ± 0.01	Class II
185	14.269 ± 0.003	12.745 ± 0.001	10.929 ± 0.001	9.14 ± 0.05	8.62 ± 0.05	8.01 ± 0.07	6.96 ± 0.20	Class I
186	14.084 ± 0.003	...	13.185 ± 0.003	13.11 ± 0.05	12.90 ± 0.09	12.49 ± 0.30	...	Field Star
187	15.49 ± 0.01	13.778 ± 0.003	12.752 ± 0.003	11.54 ± 0.05	11.10 ± 0.11	10.32 ± 0.07	...	Class II
188	...	17.57 ± 0.09	14.53 ± 0.01	Class II
189
190	15.80 ± 0.01	14.239 ± 0.004	13.280 ± 0.004	12.21 ± 0.05	11.76 ± 0.08	11.19 ± 0.10	10.51 ± 0.21	Class II
191	...	16.26 ± 0.03	14.31 ± 0.01	13.35 ± 0.06	13.09 ± 0.11	Field Star
192	15.63 ± 0.01	15.03 ± 0.01	14.31 ± 0.01	Outer-East lobe
193	16.68 ± 0.02	15.59 ± 0.01	15.12 ± 0.02	Class III
194	16.52 ± 0.02	14.41 ± 0.01	13.028 ± 0.003	11.42 ± 0.12	10.89 ± 0.18	10.29 ± 0.10	...	Class II
195	17.20 ± 0.03	15.75 ± 0.02	14.83 ± 0.01	Class II
196	...	16.65 ± 0.04	12.974 ± 0.003	Class II
197	16.90 ± 0.02	13.738 ± 0.003	11.894 ± 0.001	9.84 ± 0.04	9.08 ± 0.04	8.58 ± 0.04	8.10 ± 0.03	Class II
198	...	17.11 ± 0.06	14.42 ± 0.01	11.90 ± 0.10	10.85 ± 0.09	10.08 ± 0.08	...	Field Star
199	17.86 ± 0.05	15.38 ± 0.01	13.98 ± 0.01	12.55 ± 0.06	11.93 ± 0.07	11.41 ± 0.09	10.83 ± 0.12	Class II
200	16.55 ± 0.02	14.69 ± 0.01	13.71 ± 0.01	12.94 ± 0.08	Class III
201	18.43 ± 0.08	15.92 ± 0.02	14.61 ± 0.01	13.32 ± 0.07	12.85 ± 0.09	Class III
202	...	18.44 ± 0.20	15.24 ± 0.02	13.19 ± 0.10	12.62 ± 0.12	Field Star
203	...	18.24 ± 0.16	16.08 ± 0.04	Class II
204	16.01 ± 0.04	12.73 ± 0.07	11.47 ± 0.09	10.95 ± 0.08	Field Star
205	15.73 ± 0.01	14.088 ± 0.004	13.257 ± 0.004	12.61 ± 0.06	12.37 ± 0.20	12.09 ± 0.23	...	Class III
206	...	16.91 ± 0.05	15.38 ± 0.02	Class II
207	...	18.01 ± 0.13	15.92 ± 0.04	Class II
208	19.61 ± 0.24	15.55 ± 0.01	13.455 ± 0.004	11.59 ± 0.05	10.81 ± 0.04	10.13 ± 0.09	9.56 ± 0.16	Class III
209	...	15.45 ± 0.01	13.639 ± 0.005	12.60 ± 0.08	12.34 ± 0.10	Field Star
210	16.49 ± 0.02	15.92 ± 0.02	15.57 ± 0.03	Contamination
211	...	16.07 ± 0.02	14.42 ± 0.01	12.96 ± 0.08	12.30 ± 0.10	Field Star
212	15.23 ± 0.01	13.704 ± 0.003	12.823 ± 0.003	12.15 ± 0.06	11.74 ± 0.08	11.17 ± 0.13	...	Class III
213	13.743 ± 0.002	12.553 ± 0.001	10.980 ± 0.001	9.96 ± 0.03	9.65 ± 0.03	9.30 ± 0.05	9.08 ± 0.14	Class I
214	17.06 ± 0.02	15.20 ± 0.01	14.20 ± 0.01	13.63 ± 0.12	13.41 ± 0.14	Class III

Table 4 continued on next page

Table 4 (continued)

Source #	J	H	K _S	[3.6]	[4.5]	[5.8]	[8.0]	Type
(1)	(2)	(3)	(4)	(5)	(6)	(7)	(8)	(9)
215	16.96 ± 0.02	14.034 ± 0.004	12.553 ± 0.002	11.61 ± 0.05	11.31 ± 0.06	10.87 ± 0.12	...	Class III
216	14.715 ± 0.004	13.692 ± 0.003	13.200 ± 0.003	12.89 ± 0.15	12.66 ± 0.17	Class III
217	18.87 ± 0.12	16.92 ± 0.05	15.85 ± 0.03	Class III
218	17.70 ± 0.04	15.93 ± 0.02	14.90 ± 0.01	13.81 ± 0.11	13.55 ± 0.13	12.35 ± 0.33	...	Class II
219	18.04 ± 0.06	14.93 ± 0.01	13.027 ± 0.003	11.24 ± 0.05	10.69 ± 0.04	10.07 ± 0.10	...	Class II
220	16.97 ± 0.02	14.78 ± 0.01	13.593 ± 0.005	12.50 ± 0.18	12.10 ± 0.15	Class III
221	11.604 ± 0.001	12.306 ± 0.001	9.084 ± 0.001	8.79 ± 0.03	8.82 ± 0.05	8.75 ± 0.03	8.73 ± 0.04	Contamination
222	14.569 ± 0.003	13.922 ± 0.003	13.671 ± 0.005	13.47 ± 0.06	13.44 ± 0.11	Contamination
223	17.83 ± 0.05	15.24 ± 0.01	13.70 ± 0.01	12.41 ± 0.05	11.93 ± 0.06	11.74 ± 0.24	...	Class II
224	18.57 ± 0.40
225	16.42 ± 0.01	15.29 ± 0.01	14.78 ± 0.01	Class III
226	Galactic contamination
227	15.62 ± 0.01	14.98 ± 0.01	14.65 ± 0.01	14.13 ± 0.11	Class III
228	...	18.47 ± 0.20	...	13.80 ± 0.08	13.52 ± 0.12
229	...	18.70 ± 0.24	17.37 ± 0.13
230	17.24 ± 0.03	15.94 ± 0.02	15.26 ± 0.02	Class III
231	14.585 ± 0.004	13.927 ± 0.004	13.668 ± 0.005	13.58 ± 0.06	13.43 ± 0.09	Contamination
232	14.027 ± 0.002	13.459 ± 0.002	13.133 ± 0.003	12.89 ± 0.05	12.81 ± 0.10	12.62 ± 0.23	...	Contamination
233	AGN
234	13.509 ± 0.002	13.176 ± 0.002	12.984 ± 0.003	12.89 ± 0.06	12.87 ± 0.10	Contamination
235	16.59 ± 0.02	14.56 ± 0.01	13.559 ± 0.005	12.91 ± 0.05	12.81 ± 0.10	12.22 ± 0.23	...	Class III
236	...	18.55 ± 0.21
237	15.48 ± 0.01	14.314 ± 0.005	13.666 ± 0.005	13.26 ± 0.05	13.00 ± 0.12	Class III
238	16.85 ± 0.02	15.00 ± 0.01	14.06 ± 0.01	13.54 ± 0.08	13.35 ± 0.11	Class III
239	19.79 ± 0.29	18.12 ± 0.14	17.11 ± 0.11
240	13.886 ± 0.002	13.269 ± 0.002	13.027 ± 0.003	12.80 ± 0.06	12.95 ± 0.09	Contamination
241	14.251 ± 0.003	12.595 ± 0.001	11.379 ± 0.001	9.79 ± 0.04	9.28 ± 0.04	8.73 ± 0.03	8.20 ± 0.02	Class II
242	AGN
243	13.255 ± 0.002	12.625 ± 0.001	12.353 ± 0.002	12.21 ± 0.05	12.16 ± 0.06	11.91 ± 0.14	...	Contamination
244	...	18.01 ± 0.13	16.07 ± 0.04	Class II
245	14.153 ± 0.003	13.034 ± 0.002	12.427 ± 0.002	11.96 ± 0.05	11.87 ± 0.06	11.64 ± 0.10	...	Class III
246	16.18 ± 0.01	15.58 ± 0.01	15.26 ± 0.02	Contamination
247	18.30 ± 0.08	16.51 ± 0.03	15.59 ± 0.03	Class III
248	Galactic contamination
249	17.72 ± 0.04	16.21 ± 0.03	15.37 ± 0.02	Class III

Table 5. Subcluster Structure Properties

Subcluster	R.A. (J2000)	Dec. (J2000)	A_{hull} (pc 2)	R (pc)	σ_{hull} (pc $^{-2}$)	Total YSOs	Class I	Class II	Class III	Unclassified	Class II/ Class I	Class III/ Class II
(1)	(2)	(3)	(4)	(5)	(6)	(7)	(8)	(9)	(10)	(11)	(12)	(13)
A	16 59 18.93	-40 06 35.5	5.38	1.31	7.25	39	2	25	9	3	12.50	0.36
B	16 59 22.89	-40 10 15.6	3.91	1.12	9.20	36	6	20	7	3	3.33	0.35
C	16 59 29.10	-40 08 09.1	3.67	1.08	6.27	23	0	8	12	3	∞	1.50
D	16 59 29.39	-39 58 41.2	4.22	1.16	5.45	23	4	14	5	0	3.50	0.36
E	16 59 32.00	-40 04 03.7	2.57	0.90	6.62	17	0	11	6	0	∞	0.55
F	16 59 34.06	-40 11 38.6	3.59	1.07	9.48	34	1	23	6	4	23.00	0.26
G	16 59 39.70	-40 03 12.5	1.52	0.70	11.86	18	3	10	5	0	3.33	0.50
H	16 59 42.40	-40 03 43.9	1.30	0.64	15.40	20	0	8	1	10	∞	0.13
I	16 59 44.85	-40 00 30.9	2.89	0.96	6.93	20	3	13	3	1	4.33	0.23
J	16 59 49.37	-40 04 10.4	4.51	1.20	4.66	21	1	13	7	0	13.00	0.54
K	16 59 52.02	-40 09 20.5	3.06	0.99	4.90	15	10	5	0	0	0.50	∞

Table 6. Subcluster Average X-Ray Properties

Subcluster	N_H 10^{22} (cm $^{-2}$)	kT (keV)	EM (cm $^{-3}$)	$F_{x,c}$ 10^{-14} (erg cm $^{-2}$ s $^{-1}$)	$\log L_{x,c}$ (erg s $^{-1}$)	reduced χ^2
(1)	(2)	(3)	(4)	(5)	(6)	(7)
A	$0.65^{+0.17}_{-0.15}$	5.93	$0.88^{+0.11}_{-0.11}$	$1.27^{+0.16}_{-0.17}$	30.64	0.77
B	$1.38^{+0.18}_{-0.18}$	10.85	$2.50^{+0.20}_{-0.20}$	$3.95^{+0.32}_{-0.34}$	31.14	0.90
C	$2.13^{+0.50}_{-0.40}$	2.00	$1.80^{+0.40}_{-0.34}$	$1.73^{+0.35}_{-0.34}$	30.78	0.83
D	$1.29^{+0.52}_{-0.40}$	5.50	$0.84^{+0.21}_{-0.19}$	$1.20^{+0.29}_{-0.28}$	30.62	0.77
E	$2.05^{+0.70}_{-0.51}$	3.16	$1.47^{+0.39}_{-0.35}$	$1.70^{+0.48}_{-0.44}$	30.77	0.67
F	$0.71^{+0.13}_{-0.11}$	8.62	$2.12^{+0.19}_{-0.19}$	$3.28^{+0.32}_{-0.31}$	31.06	0.91
G	$17.40^{+4.10}_{-3.25}$	0.69	$164.58^{+87.93}_{-58.56}$	$181.57^{+82.11}_{-82.07}$	32.80	0.63
H	$11.88^{+2.39}_{-1.96}$	2.00	$15.11^{+3.57}_{-2.93}$	$14.50^{+3.32}_{-3.15}$	31.70	0.83
I	$1.01^{+0.27}_{-0.22}$	8.62	$0.38^{+0.06}_{-0.06}$	$0.59^{+0.09}_{-0.09}$	30.31	0.78
J	$2.61^{+0.36}_{-0.31}$	3.84	$2.28^{+0.29}_{-0.28}$	$2.88^{+0.35}_{-0.36}$	31.00	0.65

Table 7. Age and Disk Fraction Estimates for Each Subcluster

Subcluster	N _{tot}	N _{Age}	Median	Median	N _{diskfrac}	N _{disk}	N _{diskless}	Disk Fraction	
			(J-H)	Age (Myr)					
(1)	(2)	(3)	(4)	(5)	(6)	(7)	(8)	(9)	
A	39	34	1.41	1.59 ^{+1.41} _{-0.64}	36	27	9	0.75	
B	36	24	1.87	1.02 ^{+1.08} _{-0.35}	33	26	7	0.79	
C	23	19	1.44	1.53 ^{+1.52} _{-0.63}	20	8	12	0.4	
D	23	9	1.25	1.86 ^{+1.69} _{-0.86}	23	18	5	0.78	
E	17	15	1.76	1.07 ^{+1.13} _{-0.37}	17	11	6	0.65	
F	34	28	1.68	1.12 ^{+1.13} _{-0.37}	30	24	6	0.8	
G	18	15	1.88	1.02 ^{+1.03} _{-0.35}	18	13	5	0.72	
H	20	8	2.49	0.77 ^{+0.83} _{-0.27}	9	8	1	0.89	
I	20	14	2.02	0.96 ^{+0.99} _{-0.36}	19	16	3	0.84	
J	21	19	1.95	0.99 ^{+1.01} _{-0.34}	21	14	7	0.67	
K	15	4	1.44	1.54 ^{+1.51} _{-0.64}	15	15	0	1	

NOTE—(1) Cluster designation. (2) Total number of YSOs in each cluster. (3) Number of YSOs having near-infrared counterparts used for the age calculation. (4) median color (J-H) for all stars having near-infrared counterparts in each cluster. (5) Median age calculated for all stars having near-infrared counterparts in each cluster. The uncertainties are the 25% and 75% quartiles of the Age_{JX} versus J-H distribution from Getman et al. (2014). (6) Number of YSOs used for the disk fraction calculation. (7) Number of YSOs with disk (Class I and Class II). (8) Number of YSOs without disk (Class III). (9) Disk fraction calculated for each cluster; see text for more details.

REFERENCES

- Benjamin, R. A., Churchwell, E., Babler, B. L., et al. 2003, PASP, 115, 953
- Bonnell, I. A., Clarke, C. J., Bate, M. R., Pringle, J. E. 2001b, MNRAS, 324, 573
- Casertano, S., & Hut, P. 1985, ApJ, 298, 80
- Cesaroni, R., Felli, M., Churchwell, E., Walmsley, M. 2005a, IAU Symp. 227, Massive Star Birth: A Crossroads of Astrophysics, (Cambridge, UK: Cambridge Univ. Press)
- Chen, B. Q., Schultheis, M., Jiang, B. W., et al. 2013, A&A, 550, A42
- Cox, A. N. 2000, Allen's Astrophysical Quantities (4th ed., New York: Springer)
- de Wit, W. J., Testi, L., Palla, F., & Zinnecker, H. 2005, A&A, 437, 247
- Feigelson, E. D., & Montmerle, T. 1999, ARA&A, 37, 363
- Flaccomio, E., Micela, G., & Sciortino, S. 2012, A&A, 548, A85
- Freeman, P. E., Kashyap, V., Rosner, R., & Lamb, D. Q. 2002, ApJS, 138, 185
- Fridriksson, J. K., Homan, J., Lewin, W. H. G., Kong, A. K. H., & Pooley, D. 2008, ApJS, 177, 465
- Garmire, G., Bautz, M.W., Ford, P.G., Nousek, J.A., & Ricker, G.R. 2003, Proc. SPIE, 4851, 28
- Getman, K. V., Feigelson, E. D., Gross, N., et al. 2005a, ApJS, 160, 353
- Getman, K. V., Feigelson, E. D., Kuhn, M. A., et al. 2014, ApJ, 787, 108
- Getman, K. V., Feigelson, E. D., & Kuhn, M. A. 2014, ApJ, 787, 109
- Gregory, P. C., & Loredo, T. J. 1992, ApJ, 398, 146
- Grosso, N., Montmerle, T., Feigelson, E. D., et al. 1997, Nature, 387, 56
- Gutermuth, R. A., Megeath, S. T., Myers, P. C., et al. 2009, ApJS, 184, 18
- Guzmán, A. E., Garay, G., & Brooks, K. J. 2010, ApJ, 725, 741
- Guzmán, A. E., Garay, G., Brooks, K. J., Rathborne, J., & Güsten, R. 2011, ApJ, 736, 150
- Guzmán, A.E., Garay, G., Rodríguez, L.F., et al. 2014, ApJ, 796, 117
- Guzmán, A.E., Garay, G., Rodríguez, L. F., et al. 2016, ApJ, 826, 208
- Haisch, K. E., Lada, E. A., & Lada, C. J. 2001, ApJ, 553, L153
- Hernández, J. A., Hartmann, L., Calvet, N., et al. 2008, ApJ, 686, 1195

- Hofner, P., Delgado, H., Whitney, B., Churchwell, E., & Hendrik Linz 2002, ApJ, 579, 95
- Hofner, P., Cesaroni, R., Olmi, L., et al. 2007, A&A, 465, 197
- Imanishi, K., Koyama, K., & Tsuboi, Y. 2001, ApJ, 557, 747
- Jose, J., Kim, J. S., Herczeg, G. J., et al. 2016, ApJ, 822, 49
- Kennicutt, R. C. 1998, ARA&A, 36, 189
- Lada, C. J., Lada, E. A. 2003, ARA&A, 41, 57
- López, C., Bronfman, L., May, J., Nyman, L.-A., & Garay, G. 2011, A&A, 534, A131
- López-Calderon, C., Bronfman, L., Nyman, L.-A., et al., 2016, A&A, 595, A88
- McKee, C. F., Tan, J. C. 2003, ApJ, 585, 850
- McInnes, L., Healy, J., & Astels, S. 2017, JOSS, 2, 11
- Meyer, M. R., Calvet, N., & Hillenbrand, L. A. 1997, AJ, 114, 288
- Minniti, D., Lucas, P. W., Emerson, J. P., et al. 2010, New Astronomy, 15, 433
- Montes, V. A., Hofner, P., Anderson, C., Rosero, V. 2015, ApJS, 219, 41
- Neuhäuser, R., & Preibisch, T. 1997, A&A, 322, L37
- Ojha, D. K., Kumar, M. S. N., Davis, C. J., & Grave, J. M. C. 2010, MNRAS, 407, 1807
- Oskinova, L. M., Steinke, M., Hamann, W. -R., Sander, A., Todt, H., & Liermann, A. 2013, MNRAS, 436, 3357
- Preibisch, T., & Neuhäuser, R. 1995, Lecture Notes in Physics, Properties of X-ray flares on young stars, Flares and Flashes, ed. J. Greiner, H. W. Duerbeck, R. E. Gershberg (Springer, Berlin, Heidelberg), Vol. 454
- Rieke, G. H., & Lebofsky, M. J. 1985, ApJ, 288, 618
- Rosero, V., Hofner, P., Claussen, M., et al. 2016, ApJS, 227, 25
- Rots, A. H. 2006, ADASS XV, ASP Conference Series, ed. C. Gabriel, C. Arviset, D. Ponz, & E. Solano, 351
- Soto, M., Barbá, R., Guntherdt, G., et al. 2013, A&A, 552, A101
- Siess, L., Dufour, E., & Forestini, M. 2000, A&A, 358, 593
- Tan, J. C., Beltrán, M. T., Caselli, P., et al. 2014, Protostars and Planets VI, ed. H. Beuther, R. S. Klessen, C. P. Dullemond, and T. Henning (University of Arizona Press, Tucson), 149
- Townsley, L. K., Broos, P. S., Garmire, G. P., et al. 2014, ApJS, 213, 1
- Weisskopf, M. C., O'Dell, S., & Van Speybroeck, L. P. 1996, Proc. SPIE, 2805, 2
- Weisskopf, M. C., Brinkman, B., Canizares, C., Garmire, G., Muray, S., & Van Speybroeck, L. P. 2002, PASP, 114
- Zeilinger, P., Preibisch, T., Ratzka, T., Roccatagliata, & Petr-Gotzens, M., G. 2016, A&A, 585, A49
- Zinnecker, H., Yorke, H. W. 2007, ARA&A, 45, 481